Stony Brook University

Analysis of surface layer effects in spherical contact

A Dissertation Presented

by

Jae Hun Kim

to

The Graduate School

in Partial Fulfillment of the

Requirements

for the Degree of

Doctor of Philosophy

in

Materials Science and Engineering

Stony Brook University

August 2008

Stony Brook University

The Graduate School

Jae Hun Kim

We, the dissertation committee for the above candidate for the
Doctor of Philosophy degree, hereby recommend
acceptance of this dissertation.

Dr. Andrew Gouldstone – Dissertation Advisor
Adjunct Professor, Materials Science and Engineering

Dr. Sanjay Sampath – Chairperson of Defense
Professor, Materials Science and Engineering

Dr. T. A. Venkatesh
Assistant Professor, Materials Science and Engineering

Dr. Chad S. Korach
Assistant Professor, Mechanical Engineering
Stony Brook University

This dissertation is accepted by the Graduate School

Lawrence Martin
Dean of the Graduate School

Abstract of the Dissertation

Analysis of surface layer effects in spherical contact

by

Jae Hun Kim

Doctor of Philosophy

in

Materials Science and Engineering

Stony Brook University

2008

Spherical indentation is a powerful technique for the evaluation of mechanical properties. Due to its non self-similar and nondestructive nature, spherical indentation has advantages for assessment of materials exhibiting nonlinearity and bio materials. Though the Hertzian solution is applicable for extraction of the elastic properties from various materials, it is limited in complex materials, or with surface layer effects. In this thesis, selected problems with surface layer effects in spherical indentation are considered.

The first problem is the indentation of an elastic solid covered with a tensed membrane, applicable to many physiologic systems. Semi-analytical solutions are obtained relating indentation load to contact radius, as well as contact radius to depth. Good agreement is found between derived equations and results from finite element method (FEM) simulations. In addition, the effect of membrane on sub-surface stresses is shown quantitatively, compared to the classical solution.

The second problem is the indentation of an elastic bilayer, or film/substrate

system. A first-order elastic perturbation solution for spherical punch indentation on a film/substrate system is presented. FEM simulations were conducted for comparison with the analytic solution. FEM results indicate that the new solution is valid for a practical range of modulus mismatch, especially for a stiff film on a compliant substrate. It also shows that effective modulus curves for the spherical punch deviates from those of the flat punch when the thickness is comparable to contact size.

Dedicated To

My

Mother** and **Father

Table of Contents

List of Figures

Acknowledgements

This thesis owes its existence to the help, support and inspiration of many people.

I would like to express my sincere and deep gratitude to my adviser, Prof. Andrew Gouldstone for his support, guidance and encouragement during four years of this thesis's work. With his enthusiasm, inspiration and great efforts to teach, he helped me to enjoy academic research.

I am deeply grateful to Prof. Sanjay Sampath for invaluable advice and continuous interest in this investigation.

I am indebted to Prof. Chad Korach for the fruitful discussions and his important support throughout this work.

I wish to thank Prof. T.A. Venkatesh for serving on my dissertation committee on a short notice.

Dr. Brian Choi - He has been my best friend and mentor during my PhD. He was the one who first introduced me to my advisor. I appreciate his constant help and endless encouragement. I would have been lost somewhere in Old Engineering Building without him.

Dr. Yuhong Wu – She was my first office mate in Stony Brook. She had been a good teacher and close friend to me. I owe many thanks to her for continuous encouragement.

Meng Qu – Since she joined our group, we have been through a lot together. I am

sure that her passion and sense of humor would endear her to all in future career.

Maricris R. Silva – She has been a good collaborator on a biological project. I hope she would make a great progress on further research.

1. Introduction

1.1 Spherical indentation

Spherical indentation has been widely used to assess the mechanical properties of materials, mainly due to its well-known elastic solution. The problem of two elastic solids with smooth and non-conforming surfaces in contact was first accurately described by Hertz [1]. Initially inspired by the study of optical fringes induced in the gap between two glass lenses, Hertz postulated that each body in contact can be regarded as an elastic half-space loaded over a small elliptical region of its plane surface. For the specific axisymmetric case (Figure 1.1a), in which the contact region is circular with radius a, the contact pressure distribution in the circular contact area is given as an equation;

$$p(r) = p_o(1 - r^2 / a^2)^{1/2} \tag{1.1}$$

where p_o is the maximum stress at the contact center, r is radial distance and a is the contact radius. This problem has been further simplified for materials characterization. Consider an indentation of an elastic-half space by a rigid sphere of radius R with applied load P, inducing displacement h and contact radius a (Figure 1.1b). Based on Hertz's work, a relatively simple equation formulating relation between total load, contact radius and displacement (Hertzian equation) can be given as

$$P = \frac{8ah\mu}{3(1-\nu)} \tag{1.2}$$

where μ is shear modulus and ν is Poisson's ratio [2].

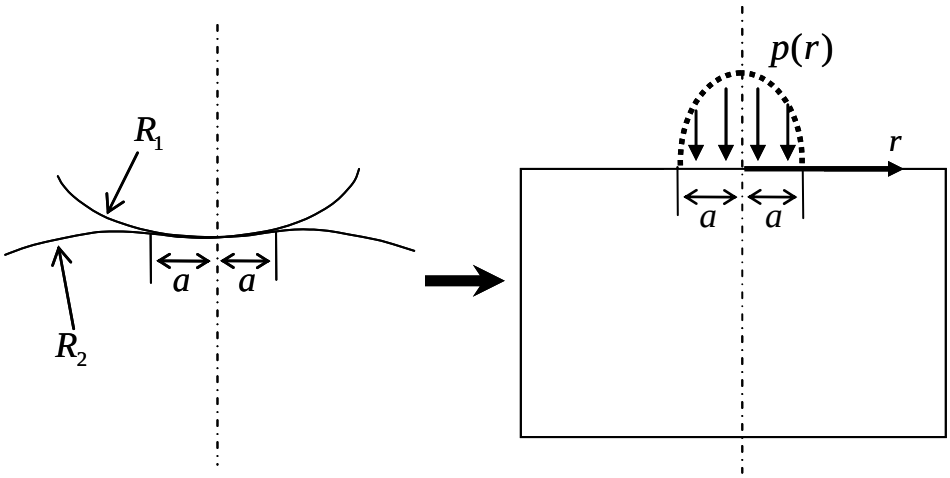

(a)

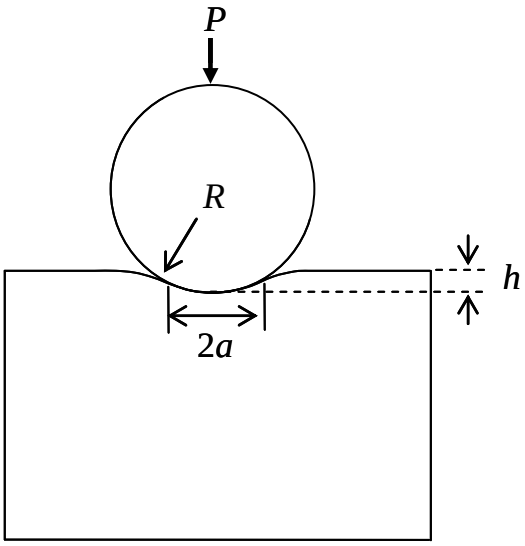

(b)

Figure 1.1 (a) Hertz's postulation: each body in contact can be regarded as an elastic half-space loaded on contact region. R_1 and R_2 are curvatures of bodies in contact, a is contact radius, and $p(r)$ is distributed pressure in contact area. (b) Schematic of indentation with a rigid sphere of radius R.

This general relation is applied to spherical indentation within the small strain range, and without friction. It is well known that this equation is accurate in the range $a/R < 0.1$ and reliable in the range $a/R < 0.2$ with maximum error of 4%.[3] Further, as the relationship between a and h is based on the geometry of the spherical tip, an equation relating force to displacement is found as

$$P = \frac{8\sqrt{R}h^{3/2}\mu}{3(1-\nu)}, \tag{1.3}$$

which is commonly used [2].

In contact characterization of materials, the two main tips in use are spherical and sharp (defined by included angle b). Vickers and Knoop hardness tests are performed with sharp tips. To relate indentation measurement to intrinsic mechanical properties, spherical indentation has several advantages compared to sharp indentation. First, whereas sharp indentation introduces a discontinuity at the tip and thus immediate inelasticity, spherical indentation gives a gradually increasing stress, allowing purely elastic deformation for shallow depth indentations (Figure 1.2) [2]. In addition, the well-defined stress fields allow onset of inelasticity to be probed [4, 5]. Second, unlike sharp indenter, a sphere does not have a self-similar geometry; a/R or characteristic strain varies with load [6], allowing measurement of stress-strain behavior including parameters like yield strength and hardening coefficient [7, 8]. Note however that sharp indentation is thus more appropriate for examining material length-scale effects.

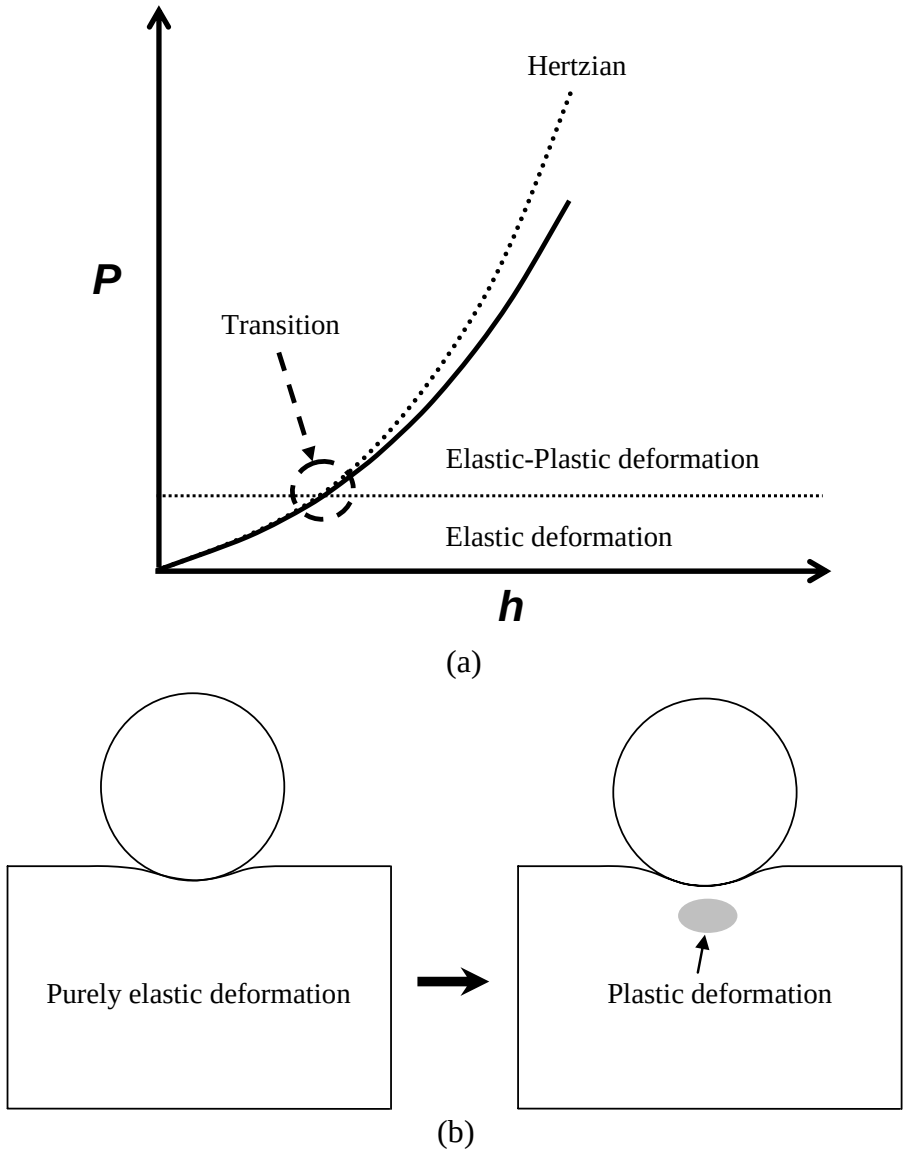

Figure 1.2 Transition between the purely elastic and the elastic-plastic deformation in spherical indentation: (a) Typical P-h curve with transition. (b) Schematic of evolution of plastic deformation. Beyond the elastic limit, plastic deformation initiate below the surface where the shear stress is the maximum.

1.2 Modulus measurement with indentation

Indentation is a popular mechanical test for modulus measurement due to its relative experimental simplicity. Initially, indentation was performed with dead-weight loading for the hardness test. In 1948, Tabor [9] first attempted to measure modulus with a spherical indenter by observing the residual impression after single load indentation. Instrumented indentation, which allows continuous load and depth measurement, was developed in the 1970's [10]. This technique has been extensively used for acquiring elastic modulus of various material systems, by examining the slope of the *unloading* P-h relation [11-15]. This analysis is well-suited for metals and other materials for which inelastic deformation does not affect elastic modulus, but for many systems, purely elastic deformation is necessary to characterize elastic behavior [16-18]. Specifically, recent attention has focused on contact probing of soft biomaterials (e.g., tissue) [19-21].

The indentation measurement of modulus is based on the known elastic solution, relating the load, displacement and contact area (Eq. 1.2). Though this equation has been successfully used for many material systems, it has limited applicability to non-homogeneous systems. Since indentation is a surface measurement technique, any surface or surface layer involved effect give a deviation from the homogenous solution. Surface effects including adhesion between an indenter and a surface, friction and surface residual stress have been studied with analytical and experimental approaches [22-25]. Surface measurement of thin films on substrates has been reported to give continuous variation of indentation modulus depending on the depth compared to the film thickness [11, 26]. Similarly, a membrane covering a soft bio-material will induce size effect on the

indentation measurement [20]. For those complex systems, a modification to Eq. (1.2) is required.

1.3 A membrane on a soft biomaterial

Indentation is attractive for probing biomaterials, largely due to the lack of necessary specimen preparation, allowing quick *in-vitro* or *in-vivo* mechanical tests, for physiologic study or possibly diagnosis (note that palpation could be considered a type of indentation). Biomaterial systems such as human brain, lung, kidney, skin, and cell have been assessed for mechanical properties, with indentation technique [15, 19-21, 27].

Indentation of ‘soft’ biomaterials raises some issues to be considered for analysis and/or property extraction, including viscoelasticity, adhesion due to moist surfaces, and structural heterogeneities in tissue samples. In the context of contact mechanics, this presents a number of problems to be solved. Among others, the size effect induced by a membrane on the surface of an organ is an interesting feature. As an example, human lung has long been considered as an elastic solid bounded by a membrane on the surface [28]. Here, the membrane is a thin layer with negligible bending rigidity. The overall mechanical properties of the lung could be obtained through indentation based on the classical elastic solution, assuming it being a homogeneous elastic solid. However, this assumption is reported to induce some error depending on the inflation pressure and the size of the indentation.[20] This membrane effect on indentation measurement is due to the in-plane prestress (membrane tension), which is usually developed in bio-membrane. The membrane imposes a size effect during contact(Figure 1.3) , that is to say, a

relatively large contact dimension 'feels' the underlying solid (relationship between indentation load P and contact radius a more so reflects the solid properties), whereas a smaller contact is more strongly affected by the membrane (depends on membrane tension compared to modulus) [20]. The relation between indentation variables (P, a and h) and membrane tension is essential to the indentation measurement for a biomaterial with tensed membrane. Inspired by the application of indentation to soft biomaterials, the problem of spherical indentation on an elastic half-space with tensed membrane on the surface is considered in this thesis. The problem definition and approach are described in detail in Chapter 4.

1.4 A thin film on a substrate

Measurement of mechanical properties of films deposited on substrates has long been an issue in thin- and thick-film technology. Although indentation is extensively used for the measurement of film due to its relative experimental simplicity, analysis is complicated by the inevitable substrate effect. Rules of practice exist that film properties may be isolated if contact dimensions are small compared to film thickness, but such simplifications are not useful for layers including microstructural size effects, or ultra-thin films. Thus, analyses that consider the relation between film and substrate properties are necessary.

Consider the indentation of an ideally elastic film/substrate system that is mechanically bonded. A proper description of the effective modulus μ_{eff} of the film/substrate system, in the context of film and substrate moduli (μ_f and μ_s) is essential

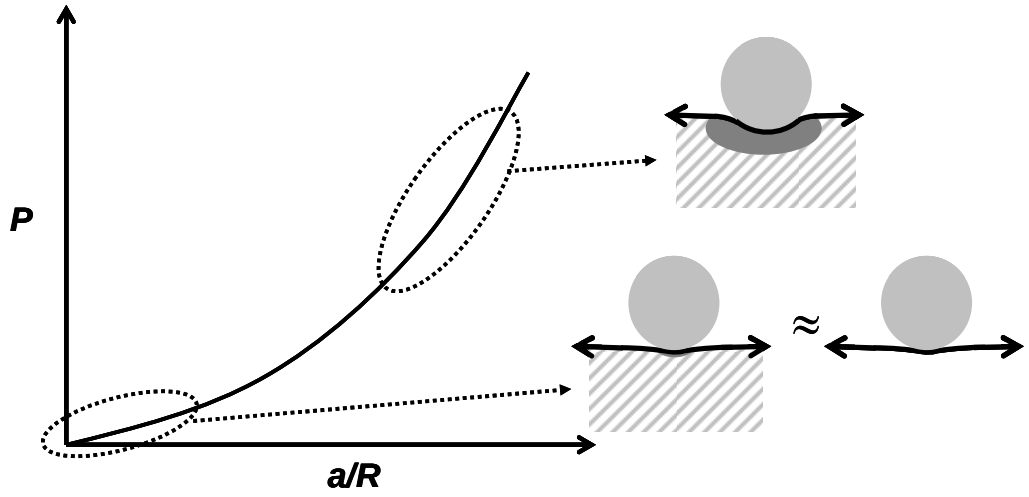

Figure 1.3 Membrane induced size effect. The effect of membrane becomes less dominant as the contact size increases.

to the accurate extraction of the film properties. Since there is no exact solution yet for this problem, a number of approximate models have been proposed to be fitted with data from experiments, FEM simulations, or analytic solutions for several tip geometries. Those models have shown good yet limited applicability. Most of these approaches were based on the following simple formula:

$$\mu_{eff} = \mu_s + (\mu_f - \mu_s)\phi(a/t, \mu_f/\mu_s) \tag{1.4}$$

where a is contact radius, t is the thickness of the film and ϕ is a weight function of contact size, tip geometry and modulus mismatch; ϕ approaches 1 when $a/t \to 0$ and 0 when $a/t \to \infty$. Numerous forms of Eq. (1.4) have been proposed for sharp and flat-ended cylindrical tip geometry. Doerner and Nix [11] first introduced an empirical equation of an effective modulus expressed as an exponential form and fit it with experimental data obtained with a sharp tip. King[29] performed a numerical analysis of flat-ended tip indentation and introduced a similar equation to Doerner and Nix's. Jung et al.[30] developed a power law function based on their experimental results from nanoindentation with ceramic films on silicon substrates.

In 1992, Gao et al.[31] performed a first order perturbation analysis on the flat-ended cylindrical punch problem, and presented a formula for effective modulus μ_{eff}. Mencik, et al.[32] compared this and several empirical equations with experimental data from nanoindentation, and found that Gao et al.'s equation gave the best fit to their experimental data. Though the perturbation approach has been confirmed to be useful for the indentation measurement on thin films, the flat punch assumption originally adopted for simplicity put a limit on its application to commonly used tip geometry, a sphere. The spherical tip indentation on a film/substrate system is considered in this thesis with a

perturbation approach. A detailed description of the problem and approach is presented in Chapter 5.

2. Statement of the Problem

Spherical indentation is used very commonly to probe mechanical behavior of a number of engineering and biological systems. The ease of implementation, availability of various tips, and non-singular stress fields make it attractive for materials, in particular where damage is to be avoided, or onset of inelasticity assessed. However, in contrast to other indenter tips, the sphere is not self-similar. That is to say, characteristic strain underneath the tip varies as contact radius changes. This can make analysis difficult. In addition, in relevant systems, surface layer effects are omnipresent, and these include thin films on substrates, thick coatings, or biological tensed membranes. There have been a number of empirical, engineering-based techniques or rules-of-thumb devised to simplify analyses in light of this, mostly adopting a strategy of avoidance. For example, it is known that if one indents a film on a substrate, one should keep contact dimensions smaller than approximately one-tenth of the film thickness, to avoid substrate effects. However, in many real cases, this is impractical, and leads to complexities of a higher level that stem from microstructural size effects. Thus, it is important to devise closed-form, accurate analyses for the spherical indentation of materials with surface layer effects, if properties are to be extracted.

In this thesis, two distinct scenarios are analyzed. In the first, inspired by biomaterials an elastic solid bounded by a tensed membrane of infinitesimal thickness is considered. In Chapter 4, spherical indentation load-depth relations are derived in a general manner. With the help of FEM, the Hertzian boundary condition is modified to accommodate the effect of membrane. Analytical models are compared with FEM

calculations. The subsurface stress is studied compared to classical model. In the second scenario, the problem of an elastic film on an elastic substrate is revisited. Indentation modulus of film/substrate system depends on the contact geometry, and also the shape of the tip. In Chapter 5, spherical indentation of the composite material is analyzed using a modified perturbation approach first adopted by Gao, et al [31] for the indentation problem. When compared with FEM, this analysis is shown to be particularly accurate in the case of a stiff film on a compliant substrate, which is the case in a large percentage of engineering applications. The FEM results with different tips are compared to show the effect of tip geometry on the composite modulus.

3. Finite Element Simulation

3.1 Introduction

Finite element method (FEM) simulation has been used extensively for contact mechanics problems. Other than indentation with homogeneous material, this technique allows analysis of indentation problems with complicated systems such as layered, graded and cracked materials [33-35].

In this thesis, FEM is used to validate analytic predictions. All the simulations were performed using commercial code ABAQUS [36]. Two different models have been developed in this study. Both are modeled as axisymmetric and elastic solids. Mesh convergence was checked with classical elastic equations for each geometry assuming homogeneous material. The mesh was refined until the error compared to the equation was less than 1%.

3.2 Finite element models and boundary conditions

3.2.1 Spherical indentation of a membrane on an elastic half-space

Figure 3.1 shows a schematic of the model used in Chapter 4. The spherical indenter was modeled as a rigid surface with $R = 10$. The elastic solid was modeled as an isotropic, two-dimensional solid using four-noded axisymmetric quadrilateral elements (29945 total). Two-noded axisymmetric membrane elements (1090 total) were used to simulate the membrane on top of the elastic solid.

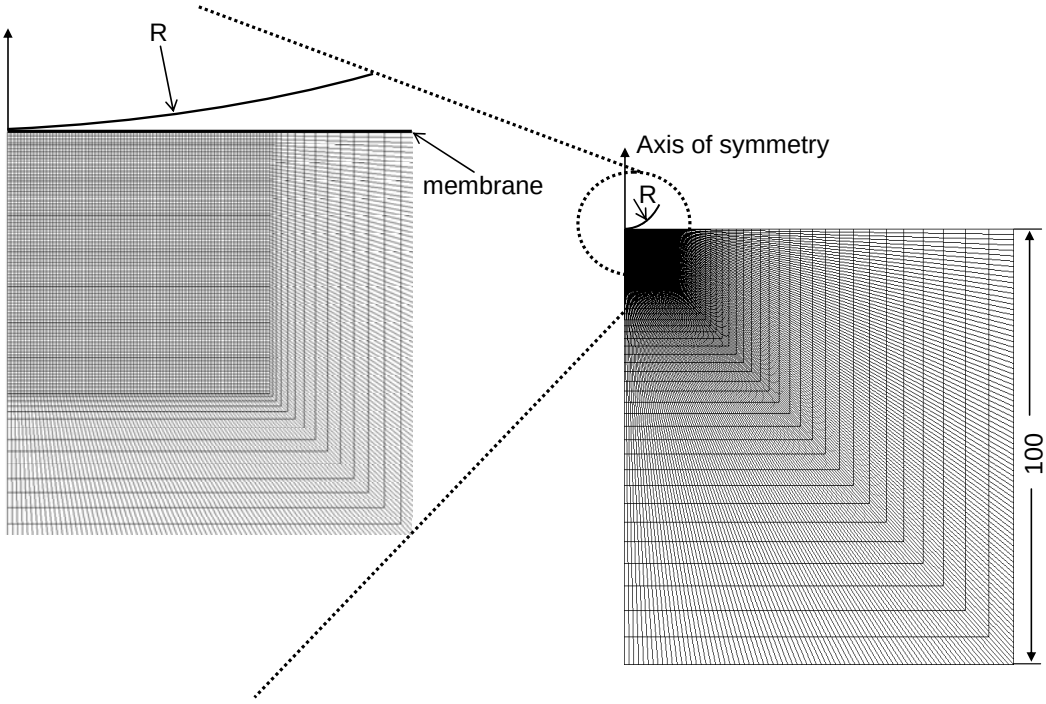

Figure 3.1 Finite element model of spherical indentation on an elastic solid with membrane.

To exclude the effect of Poisson's ratio and membrane thickness change under indentation, the membrane was assigned a Poisson's ratio of 0.4999 and a thickness of $10^{-4}R$. Membrane tension was imparted via artificial thermal strains; to ensure near-constant T_o during indentation, membrane modulus was low and imposed strains were accordingly high (effect of input modulus had no effect on results). Attachment between membrane and solid was imposed via the 'friction' option, after tensing. All models were performed allowing for large deformation.

3.2.2 Spherical indentation of an elastic bilayer

Figure 3.2 shows a model used in Chapter 5. The spherical indenter was modeled as a rigid surface with $R = 20$, and the film and the substrate were modeled as elastic solids bonded to each other. Maximum displacement was set to a limit such that $a/R \le 0.05$. Film thickness t was varied between 0.005 and 6 to determine effective modulus in the range $0.02 \le a/t \le 100$. The film/substrate system was modeled with small quadrilateral elements of length 0.0075 near the contact region for the accurate measurement of contact radius a. Poison's ratio was fixed at 0.3 for the film and the substrate. In addition, flat punch indentation was simulated with variable thickness of the film for comparison to spherical punch. Figure 3.3 shows a model for flat punch indentation. The film/substrate system was modeled with small elements near the contact area similarly to the model for spherical punch indentation.

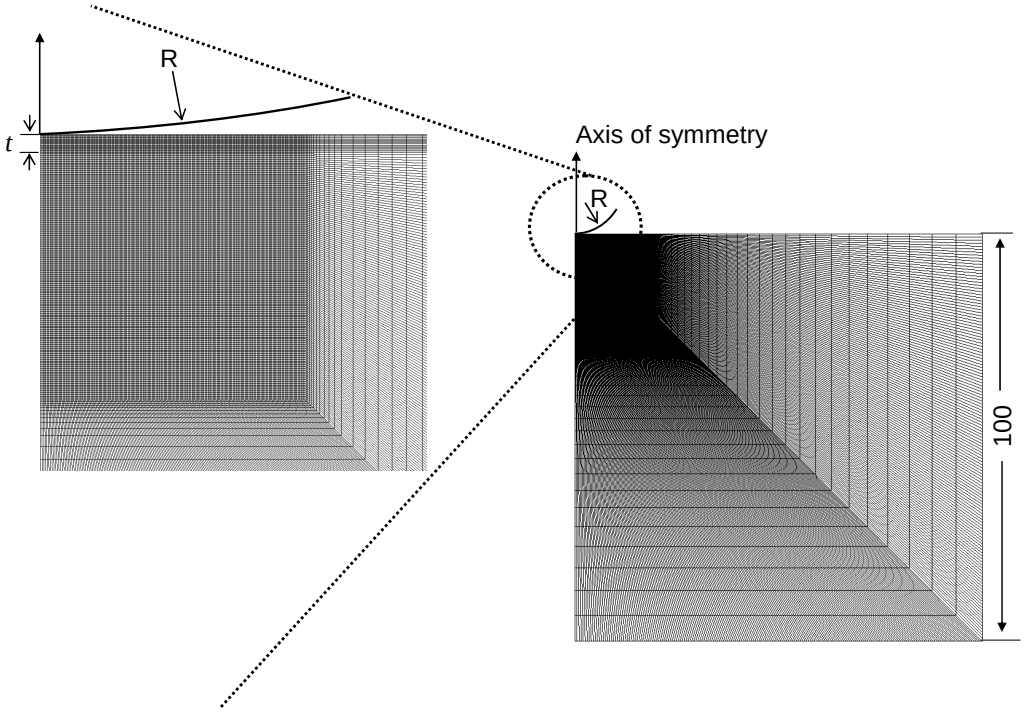

Figure 3.2 Finite element model of spherical indentation on an elastic film/substrate system.

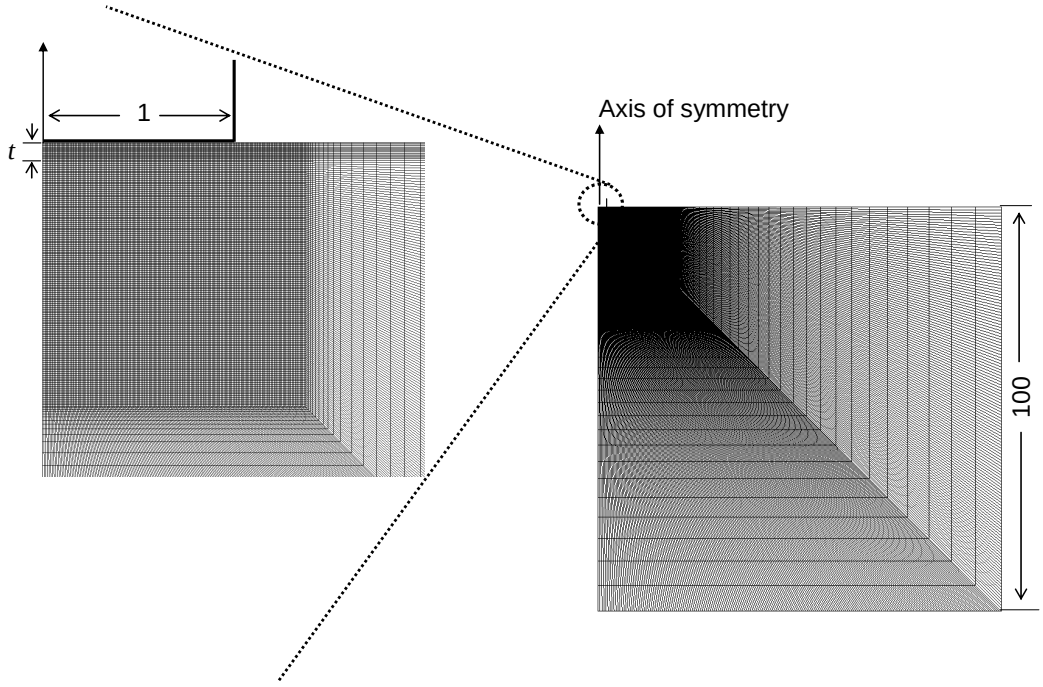

Figure 3.3 Finite element model of flat punch indentation on an elastic film/substrate system.

4. Spherical Indentation of A Membrane on An Elastic Half-Space

4.1 Introduction

In this chapter, a problem of spherical indentation of an elastic half-space, covered with a tensed membrane, is addressed. This is equivalent to indentation of an elastic thin plate/film on an elastic solid, where the thickness and stiffness of film are sufficiently small to neglect bending rigidity [37]. This problem arises in a few instances, some examples being contact of the lung, which can be treated as a quasi-elastic solid surrounded by a thin [pleural] membrane, or other viscera, or skin over muscle or fat. Spherical indentation of these systems would be useful in the extraction of material properties for modeling purposes, or for physiology and diagnosis. Here, a quantitative description of this is approximately derived, relating P to a, using material properties and indenter geometry as input. In addition, sub-surface stress fields are presented. Results are compared with FEM results, and ranges of applicability are discussed.

Figure 4.1 displays a schematic of the problem to be solved – a spherical indenter of tip radius R is pressed into a linear elastic half-space (shear modulus μ and Poisson's ratio ν) covered with a tensed membrane (constant tension T_o). The assumption of no time-dependent behavior is necessary for a tractable solution here. However, this may be incorporated into the solution by substituting viscoelastic operator for the modulus [38]. Contact between indenter and membrane is frictionless.

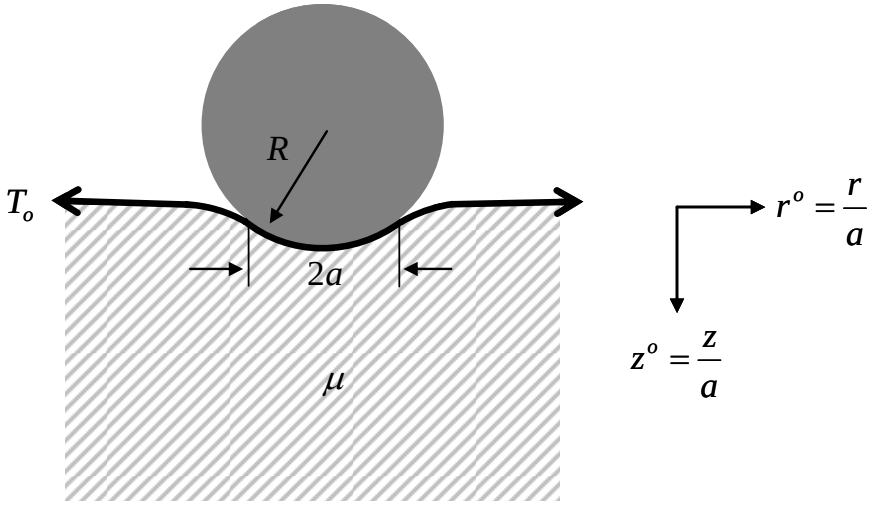

Figure 4.1 Schematic of the problem to be addressed.

In the present solution, the membrane is considered to be freely sliding on the solid (detachment may not occur). In a real case, the membrane would be fully attached, but it is shown later that for $P-a$ relations, within small strains our solution describes this case well.

Similar problems of (i) a circular area of constant pressure p_o, or (ii) a rigid flat punch acting upon the half-space/membrane system were addressed analytically by Hajji [39] and numerically by Gouldstone et al. [40] , respectively. Both of these investigations were motivated via mechanical investigation of respiratory organs, and are well-suited for the measurement of, e.g., elastic properties of the probed specimens. The reasons for addressing this problem further here, i.e., with a spherical indenter, include the following:

- Method (i) does not lend itself well to systematic practical experiments (load, unload), as the pressure is applied via a column of water.
- Method (ii) potentially introduces singularities at the edge of contact.

(Thus, the above methods may not be used to examine inelastic mechanisms.)

- In order to distinguish solid and membrane properties, two or more indenters of different sizes are required.
- Indentation with a curved surface is more physiologically relevant, when considering rib/lung, heart/lung, inter-viscera contact or palpation.

Spherical indentation addresses these points, but on the other hand it is more complicated in its analysis due to the change in contact dimensions with load. As mentioned above, Hajii analytically considered the effects of membrane on indentation with a circular area of constant pressure. The spherical indentation case can be solved using similar

methods, but determination of proper surface loading conditions is non-trivial. This will be explained in the following section. In addition, after solving for *P-a* relations, sub-surface stress fields, that are very important for investigation of inelastic mechanisms, are discussed.

4.2 Modified boundary condition

We approach the problem by first considering the boundary conditions on the surface of the membrane (Figure 4.1). The solid is considered to be isotropic linear elastic, with shear modulus μ and Poisson's ratio ν. Membrane behavior is given by

$$p = T_i k_i \tag{4.1}$$

where p, T_i and k_i are pressure, tension and curvature, respectively. In Hajji's case, he applied a pressure boundary condition on the surface, and solved the corresponding stress functions. For a sphere indenting the surface of a half-space, Sneddon [41] showed that a mixed boundary condition could be used:

$$\begin{aligned} &\tau_{rz}(r,0) = 0 \\ &u_z(r,0) = h - f(r/a), \quad r \le a \\ &\tau_{zz}(r,0) = 0, \quad r > a \end{aligned} \tag{4.2}$$

where f is an equation for punch shape, and h is indentation depth. However, the existence of the membrane complicates this, in that normal stress is non-zero outside the region of contact (see Figure 4.2a). On the other hand, Hertz [1] used a pressure boundary condition for the surface of an elastic solid, given as:

$$\tau_{zz}(r,0) = p_c(r) = p_o\left(1-\frac{r^2}{a^2}\right)^{1/2}, \quad r \le a \tag{4.3}$$

where $p_c(r)$ is contact pressure and p_o is maximum pressure. Contribution from the tensed membrane has the following effects. Figure 4.2 shows the normalized Hertzian pressure distribution for an elastic solid, compared with that obtained from a sample FEM calculation in which the solid is covered with a tensed membrane (see section 3.2.1 for methods). Two main differences arise. First, as stated above, in the latter case the surface pressure on the solid is non-zero outside of the contact perimeter. This is due to the non-zero curvature of the membrane. Second, the slope of the surface pressure distribution is not infinity at the contact perimeter (Figure 4.2b). The pressure distribution in Eq. (4.3) must be modified to reflect these differences. Briefly, the pressure on the surface of the membrane due to spherical contact can then be obtained via superposition of two terms: (i) the corrected Hertzian pressure on the surface of the solid and (ii) the pressure in the contact region due to membrane curvature. The normal pressure distribution between a sphere and membrane in contact was suggested by Yang [42] to be

$$p_n(r) = 2\frac{T_o}{R}, \quad r \le a \tag{4.4}$$

where T_o is stretch-independent membrane tension, R is radius of the spherical tip. By inspection, we found that Eq. (4.3) could be modified to an approximate form in the following manner:

$$p_c(r) = p_o\left(1-\frac{r^2}{(a\cdot b)^2}\right)^{1/2} + C + 2\frac{T_o}{R}, \quad r \le a \tag{4.5}$$

where b is included to modify the shape of pressure distribution, and C is the pressure difference between the Hertzian pressure and the surface pressure with tensed membrane,

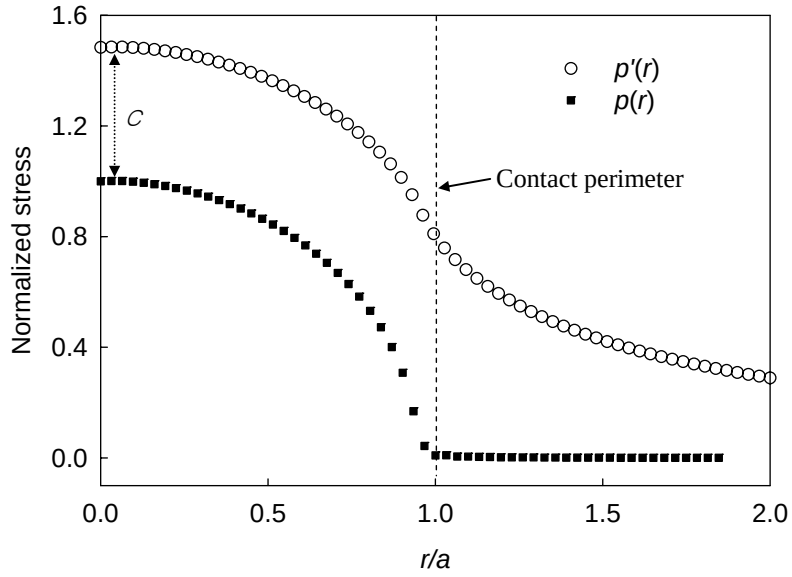

(a)

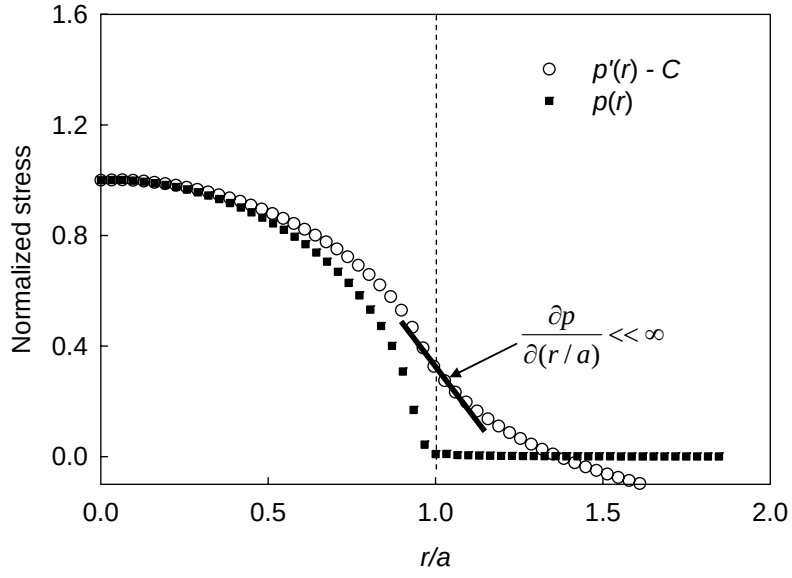

(b)

Figure 4.2 Stress distribution on the surface of elastic solid as shown from FE simulation; (a) $p'(r)$: stress with membrane effect, $p(r)$: stress without membrane effect, (b) $p'(r) - C$: stress distribution subtracting C.

at $r/a = 0$ in Figure 4.2a. Essentially, these constants are required to maintain the spherical geometry in the contact region. Analytical determination of the constant b is non-trivial, so we found it numerically by fitting the surface pressure distribution obtained by FEM for a range of moduli, tension and contact dimensions. Figure 4.3 shows the dependency of b on membrane tension normalized by shear modulus and Poisson's ratio. It can be seen that b increases from 1 to 1.11 as membrane tension increases, without dependence on dimensional parameter, radius or material parameters. The relation between b and tension normalized by modulus and Poisson's ratio can be fitted with the hyperbolic equation

$$b = A_1 - \frac{A_2}{(1 + A_3 \cdot T_o(1-\nu)/\mu)^{1/A_4}} \tag{4.6}$$

where A_1, A_2, A_3, A_4 are constants (see Appendix 1). The constant C is not obtained via simulation, but falls out of the equations; this will be addressed in a section 4.4. It can be shown that this boundary condition is applicable whether the membrane is attached to the solid, or free standing, for small contact dimensions a/R. With an appropriate approximate surface pressure condition, we now follow a variation on Hajji's method to obtain resulting stress and displacement fields.

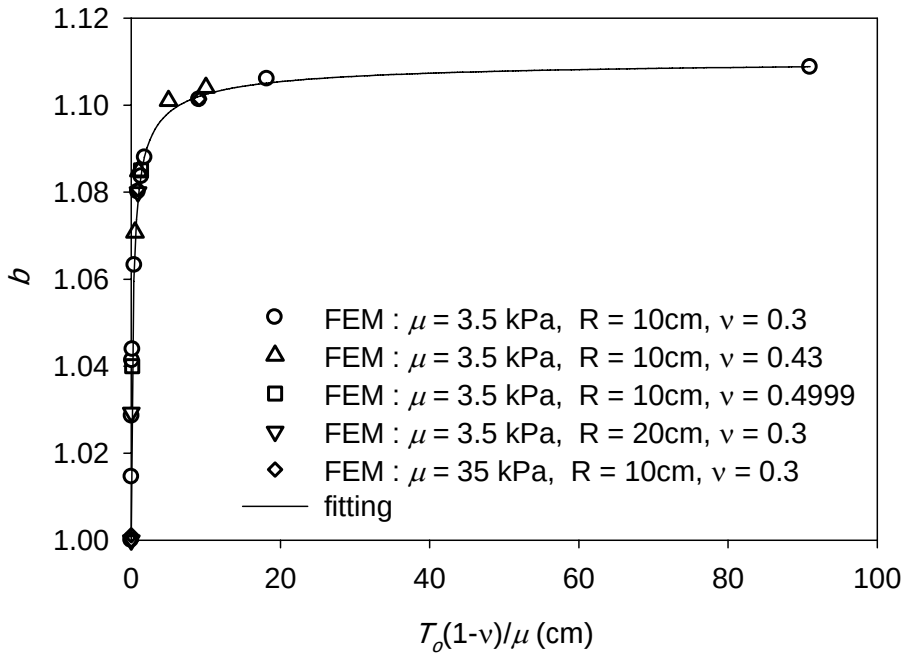

Figure 4.3 Modification constant b vs. normalized tension. The constant varies with membrane tension effect following hyperbola relation, but independent of geometry of contact and material parameters.

4.3 Elastic solution for axisymmetric problem

In this section, the elastic solution of the axisymmetric problem is derived following the approach used by Hajji [39]. Without body forces, the classical elastic equilibrium equation, in displacement formulation is given as

$$\nabla^2 u + \frac{1}{1-2\nu}\nabla(\nabla \cdot u) = 0 \tag{4.7}$$

where u is the nondimensional displacement field of the half space, ν is Poisson's ratio and ∇ is the gradient operator in cylindrical coordinates given by

$$\nabla = \bar{e}_{r^o}\frac{\partial}{\partial r^o} + \bar{e}_{\theta}\frac{1}{r^o}\frac{\partial}{\partial \theta} + \bar{e}_{z^o}\frac{\partial}{\partial z^o} \tag{4.8}$$

where r^o and z^o are cylindrical coordinates normalized with respect to contact radius a, $\bar{e}_{r^o}$, $\bar{e}_{\theta}$, $\bar{e}_{z^o}$ are unit vectors, and ∇^2 is the Laplacian operator given by

$$\nabla^2 = \frac{1}{r^o}\frac{\partial}{\partial r^o}\left(r^o\frac{\partial}{\partial r^o}\right) + \frac{1}{r^{o2}}\frac{\partial^2}{\partial \theta^2} + \frac{\partial^2}{\partial z^{o2}} \tag{4.9}$$

If we were to consider that the membrane is in frictionless contact with the solid, the boundary conditions on the top of the half space would be

$$\tau_{z^o z^o}(r^o,0) = -p_s(r^o)/\mu \tag{4.10a}$$

$$\tau_{z^o r^o}(r^o,0) = 0 \tag{4.10b}$$

where $\tau_{z^o z^o}(r^o,0)$ is normal stress, $\tau_{z^o r^o}(r^o,0)$ is shear stress at the top of the half space, and $p_s(r^o)/\mu$ is the normalized pressure exerted by the membrane on the surface of the half space.

The torsionless axisymmetric contact problem can be solved with the Boussinesq forms,

in terms of two harmonic functions [43]. The displacement field is thus given as

$$u_{r^o}(r^o, z^o) = \frac{\partial \Phi}{\partial r^o} + z^o \frac{\partial \Psi}{\partial z^o} \tag{4.11a}$$

$$u_{\theta}(r^o, z^o) = 0 \tag{4.11b}$$

$$u_{z^o}(r^o, z^o) = \frac{\partial \Phi}{\partial r^o} + z^o \frac{\partial \Psi}{\partial z^o} - (3 - 4\nu)\Psi \tag{4.11c}$$

where Φ, Ψ are harmonic functions independent of θ,

$$\nabla^2 \Phi = 0, \quad \nabla^2 \Psi = 0 \tag{4.12}$$

Similarly, the stress field can be given as

$$\tau_{z^o z^o}(r^o, z^o) = 2\frac{\partial^2 \Phi}{\partial r^{o2}} - 4(1-\nu)\frac{\partial \Psi}{\partial z^o} + 2z^o \frac{\partial^2 \Psi}{\partial z^{o2}} \tag{4.13a}$$

$$\tau_{z^o r^o}(r^o, z^o) = 2\frac{\partial^2 \Phi}{\partial r^o \partial z^o} - 2(1-2\nu)\frac{\partial \Psi}{\partial r^o} + 2z^o \frac{\partial^2 \Psi}{\partial r^o \partial z^o} \tag{4.13b}$$

Considering that the stress and displacement field vanish at infinite distance, it is clear that Φ, Ψ and their first and second partial derivatives vanish at infinite distance from (0, 0). Based on this observation, Hajji [44] suggested that Eqs. (4.11) and (4.13) could be solved using a Hankel Transform, and with assumption of frictionless contact, the displacement and stress fields at the surface of the solid are

$$u_{r^o}(r^o, 0) = (1-2\nu)\int_0^\infty \beta(k) J_1(kr^o) dk \tag{4.14a}$$

$$u_{z^o}(r^o, 0) = -2(1-\nu)\int_0^\infty \beta(k) J_0(kr^o) dk \tag{4.14b}$$

$$\tau_{z^o z^o}(r^o, 0) = 2\int_0^\infty k\beta(k) J_0(kr^o) dk \tag{4.14c}$$

$$\tau_{z^o r^o}(r^o, 0) = 0 \tag{4.14d}$$

where J_o and J_1 are Bessel functions of orders 0 and 1, respectively, β is an

arbitrary function, and k is a transform variable.

4.4 Semi-analytic solution for membrane/solid

In this section, the elastic solution of the spherical indentation on elastic half space bounded by membrane is presented by applying modified boundary condition extracted in section 4.2 to the general solution in section 4.3. Considering the boundary condition given in Eq. (4.10a), Eq. (4.14) can be solved with surface pressure distribution, p_s, which is the same as the applied contact pressure for classical contact. Here p_s is not known *a priori* and affected by the interaction between the membrane and solid. However, with knowledge of contact pressure between the sphere and the membrane p_c (Eq. 4.5), this membrane effect on surface pressure distribution p_s, can be deduced by the governing equation for pressure equilibrium:

$$\frac{p_s(r^o)}{\mu} = \frac{T_o}{\mu a}\kappa + \frac{p_c(r^o)}{\mu} H(1-r^o) \tag{4.15}$$

where κ is the linearized curvature, p_c is the contact pressure distribution given from Eq. (4.5), and H is the Heaviside step function. If we assume that the membrane displacement has no dependency on z^o coordinate (due to its infinitesimal thickness), the linearized curvature in cylindrical coordinates can be expressed as

$$\kappa = \nabla^2 w = \frac{1}{r^o}\frac{\partial}{\partial r^o}\left(r^o \frac{\partial w}{\partial r^o} \right) \tag{4.16}$$

where w is nondimensional displacement of the membrane [45]. Since the membrane displacement w is equal to the elastic solid displacement u_{z^o} at the surface,

$$w = u_{z^o}(r^o,0) = -2(1-\nu)\int_0^\infty \beta(k)J_0(kr^o)dk \tag{4.17}$$

Substitution of Eqs. (4.5), (4.16) and (4.17) into Eq. (4.15) gives

$$\int_0^\infty [1+\varepsilon k]k\beta(k)J_o(kr^o)dk = -\frac{p_o}{2\mu}\left(1-\frac{r^{o2}}{b^2}\right)^{1/2} H(1-r^o) - \frac{1}{2\mu}\left(C+2\frac{T_o}{R}\right)H(1-r^o) \tag{4.18}$$

where ε is a normalized membrane tension parameter given as

$$\varepsilon = \frac{T_o}{\mu a}(1-\nu) \tag{4.19}$$

Equation (4.18) can be solved using Hankel transform pairs giving

$$\beta(k) = -\frac{p_o}{2\mu[1+\varepsilon k]}\int_0^1\left(1-\frac{r^{o2}}{b^2}\right)^{1/2} r^o J_o(kr^o)dr^o - \frac{1}{2\mu}\left(C+2\frac{T_o}{R}\right)\frac{J_1(k)}{k[1+\varepsilon k]} \tag{4.20}$$

The constant C can be dealt with in the following manner. The total load P can be calculated from integration of the contact pressure p_c (Eq. 4.5) in the contact region;

$$P = p_o a^2 \cdot \int_0^1\left(1-\frac{r^{o2}}{b^2}\right)^{1/2} 2\pi r^o dr^o + \pi a^2\left(C+2\frac{T_0}{R}\right) \tag{4.21}$$

Rearrangement of Eq. (4.21) gives

$$\left(C+2\frac{T_0}{R}\right) = \frac{P - p_o a^2 M}{\pi a^2} \tag{4.22}$$

where M is the elliptic integral term in Eq. (4.21) (see Appendix 2). The above may then be substituted into Eq. (4.20).

Finally, inserting Eq. (4.20) into Eq. (4.14) gives the solution for the displacement and the stress field in this problem. The normal displacement at the surface is given as

$$u_{z^o}(r^o,0)=\frac{(1-\nu)}{\mu}\left[p_o I_1(r^o)+\frac{(P-p_o a^2 M)}{\pi a^2}L_1(r^o)\right] \tag{4.23}$$

where I_1 and L_1 are integral terms (see Appendix 2). The equation for the normal displacement at the surface can be modified to extract the total load versus contact area relation using the following geometry of the spherical contact,

$$u_z(a,0)-u_z(0,0)=a\left(u_{z^o}(1,0)-u_{z^o}(0,0)\right)=\frac{a^2}{2R} \tag{4.24}$$

Substituting Eq. (4.23) into Eq. (4.24) gives the total load as a function of contact radius and elastic properties;

$$P=\frac{\mu}{(1-\nu)}\frac{a^3}{R}\cdot\left[\left(\frac{\pi}{2}-4\left(I_1(0)-I_1(1)\right)\right)/\left(L_1(0)-L_1(1)\right)+\frac{4}{\pi}\cdot M\right] \tag{4.25}$$

The penetration depth of indenter h can be calculated by substituting Eq. (4.25) into Eq. (4.23);

$$h=a\cdot u_{z^o}(1,0)=\frac{a^2}{R}\left[\left(\frac{1}{2}-\frac{4}{\pi}\left(I_1(0)-I_1(1)\right)\right)/\left(L_1(0)-L_1(1)\right)\cdot L_1(0)+\frac{4}{\pi}I_1(0)\right] \tag{4.26}$$

Both of the total load P and the depth h can be deduced from contact radius a and material parameters with Eqs. (4.25) and (4.26).

4.5 Results and discussion

From the proceeding analyses, we have derived two expressions for the load P and the depth h. For verification, these equations (4.25, 4.26) were compared with finite element models using ABAQUS [36]. The spherical indentation on an elastic half-space with tensed membrane on top was modeled as described in section 3.2.1 In keeping with

the original motivation of the work, results are shown here for Poisson's ratio $\nu = 0.43$, which has been reported for lung [20], but are valid for all values of ν. $R = 10$ in all simulations; the significance of including this value is described below.

Figures 4.4a-c shows the derived results (Eqs. 4.25, 4.26) with FEM calculations, over a range of input variables. In Figure 4.4a, data is plotted against explicit variation of the ratio $T_o(1-\nu)/\mu$, with μ held constant. Satisfactory agreement was found between Eq. (4.25) and FEM, over the a/R range shown. Not surprisingly, P increases significantly with increasing T_o. For further verification, note that the solution equals the Hertzian prediction for $T_o = 0$. Figure 4.4b shows additional variation, this time with constant $T_o(1-\nu)/\mu$ and varied μ, and again good agreement is found between analysis and FEM. Figure 4.4c compares Eq. (4.26) to results from FEM with varying $T_o(1-\nu)/\mu$, showing good agreement between the two. Note the range of tension/modulus shown in this data covers a reasonable range expected for most biomaterials (e.g. Hajji [39] and Stamenovic [46]).

It is important to recognize that the ratio $T_o(1-\nu)/\mu$ is not dimensionless, and has units of length. In Hajji's original treatment, the contact radius a was included in the denominator, removing this complexity. However, in the current analysis, a varies with depth. This results in an inherent length scale into the problem, and recognition of modeling units becomes necessary. For example, if one were to consider a membrane tension $T_o = 1000$ dynes/cm and $\mu = 1000$ dynes/cm^2, the data in Figure 4.4 would be applicable for indentation with tip radius $R = 10$ cm. If SI units were chosen ($T_o = 1000$ N/m, $\mu = 1000$ N/m^2), a tip radius of $R = 10$ m would be applicable.

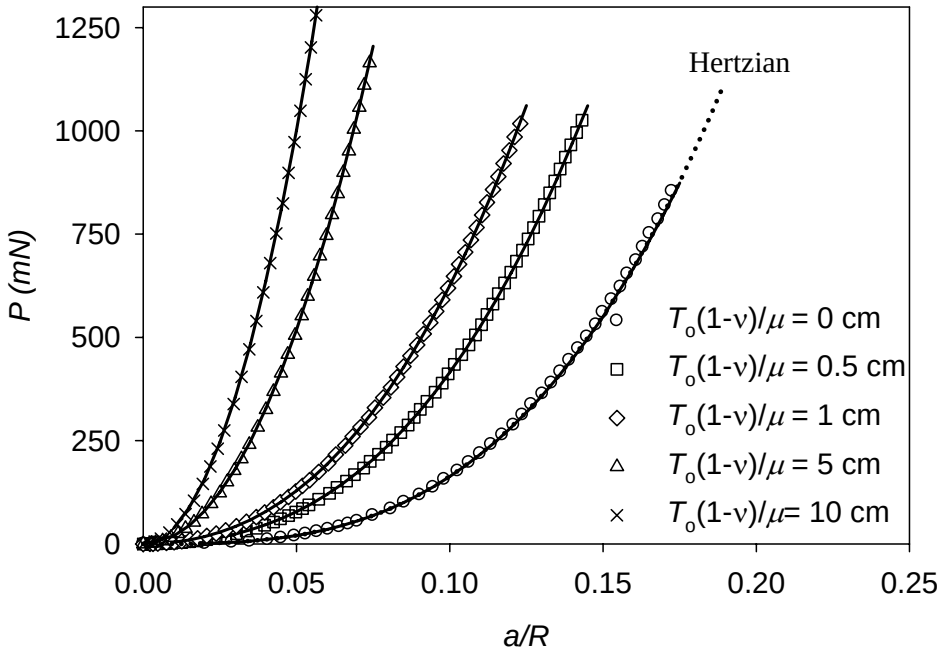
1250
1000
750
500
250
0
P (mN)
0.00
0.05
0.10
0.15
0.20
0.25
a/R
Hertzian
T0(1-ν)/μ = 0 cm
T0(1-ν)/μ = 0.5 cm
T0(1-ν)/μ = 1 cm
T0(1-ν)/μ = 5 cm
T0(1-ν)/μ= 10 cm

(a)

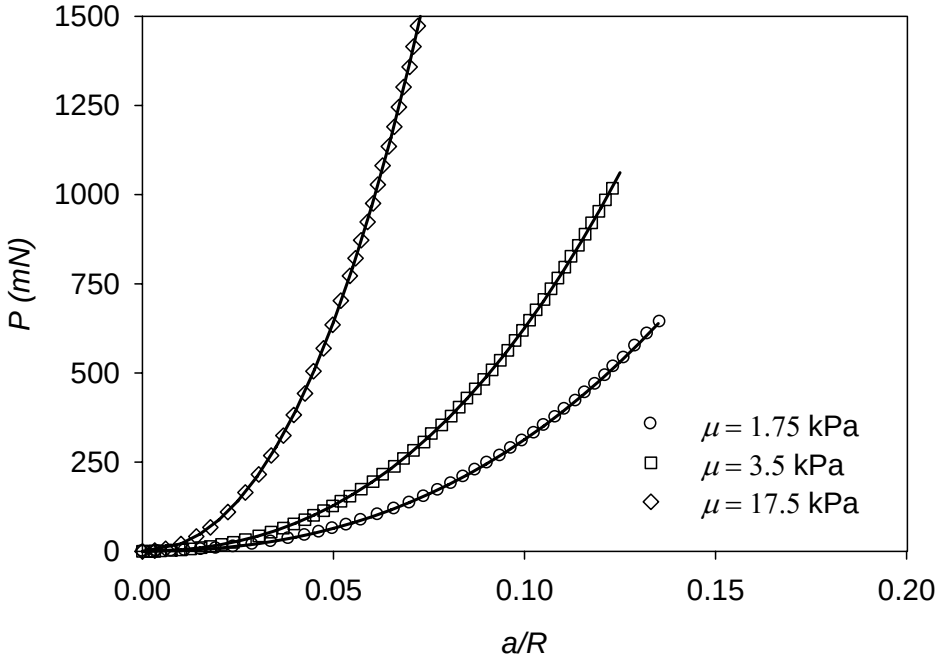
1500
1250
1000
750
500
250
0
P (mN)
0.00
0.05
0.10
0.15
0.20
a/R
μ = 1.75 kPa
μ = 3.5 kPa
μ = 17.5 kPa

(b)

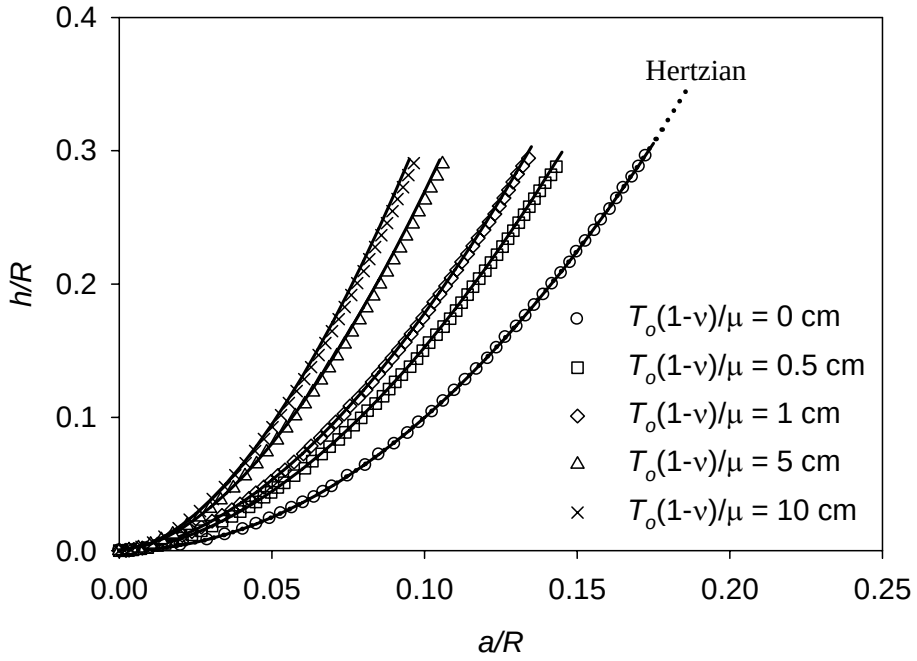

(c)

Figure 4.4 (a) Load-contact radius curves; $\nu = 0.43$, $\mu = 3.5\,kPa$, $T_o(1-\nu)/\mu$ is normalized membrane tension; (b) Load-contact radius curves with fixed membrane effect; $\nu = 0.43$, Normalized membrane tension is fixed at $T_o(1-\nu)/\mu = 1\,cm$; (c) Depth-contact radius curves; $\nu = 0.43$, $\mu = 3.5\,kPa$. Solid lines are from analytical solution, dots are from FE simulations.

In this study we have investigated systems of physiologic relevance. Thus, the Figures are plotted for a tip radius of R = 10 cm, which is of order organ size, moduli are of order kPa, and tension of order $kPa \cdot cm$.

Figure 4.5 shows comparison (for P vs a/R) between the analytical formulae treating membrane/solid contact as frictionless, and FEM calculations in which membrane was attached to solid. Data are shown for a range of solid/membrane properties, and agreement between the two solutions is very good. This result shows that within this range, the derivation presented here should be applicable for real systems, at least for determination/analysis of $P-a$. In addition, as shear stresses are ostensibly non-zero in the case of attached membrane, this result shows that $P-a$ is relatively insensitive to surface shear stresses over this range.

For analyzing, e.g., initial inelastic events, it is useful to know the distribution of, e.g., shear stresses underneath the indenter tip. Here we show selected comparisons of (i) pressure and displacement distribution at the indented surface and (ii) maximum shear stress (calculated from principals) along the axis of symmetry of indentation. The explicit relations may be calculated using Eqs. (4.14, 4.20) and are placed in the Appendix 3. Figure 4.6 shows surface distributions of normal stress and displacement, calculated via the analysis in this work, and FEM. Good agreement was found between both approaches. Note for this case, results are compared using $\nu = 0.43$, but other input values led to similar matching of analysis and FEM. Figures 4.7 a and b show distributions and location of maximum shear stress, respectively, for a range of input parameters. Figure 4.7a mimics the presentation from Johnson [2] normalizing the shear stress with respect to p_o, for a range of membrane tension.

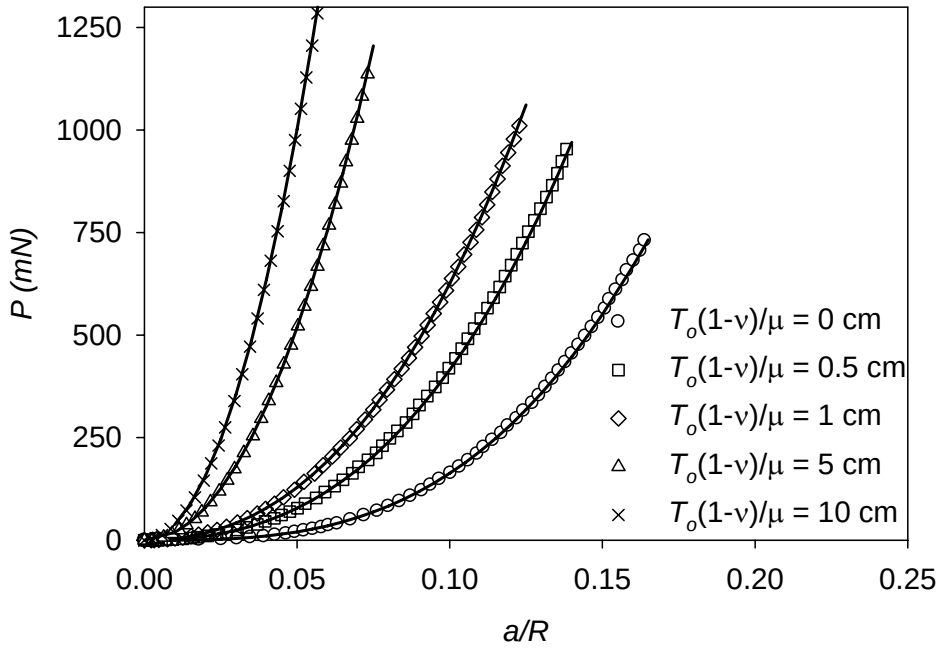

Figure 4.5 Load-contact radius curves; $\nu = 0.43$, $\mu = 3.5\,kPa$, $T_o(1-\nu)/\mu$ is normalized membrane tension; Solid lines are from analytical solution, dots are from FE simulations with membrane attachment.

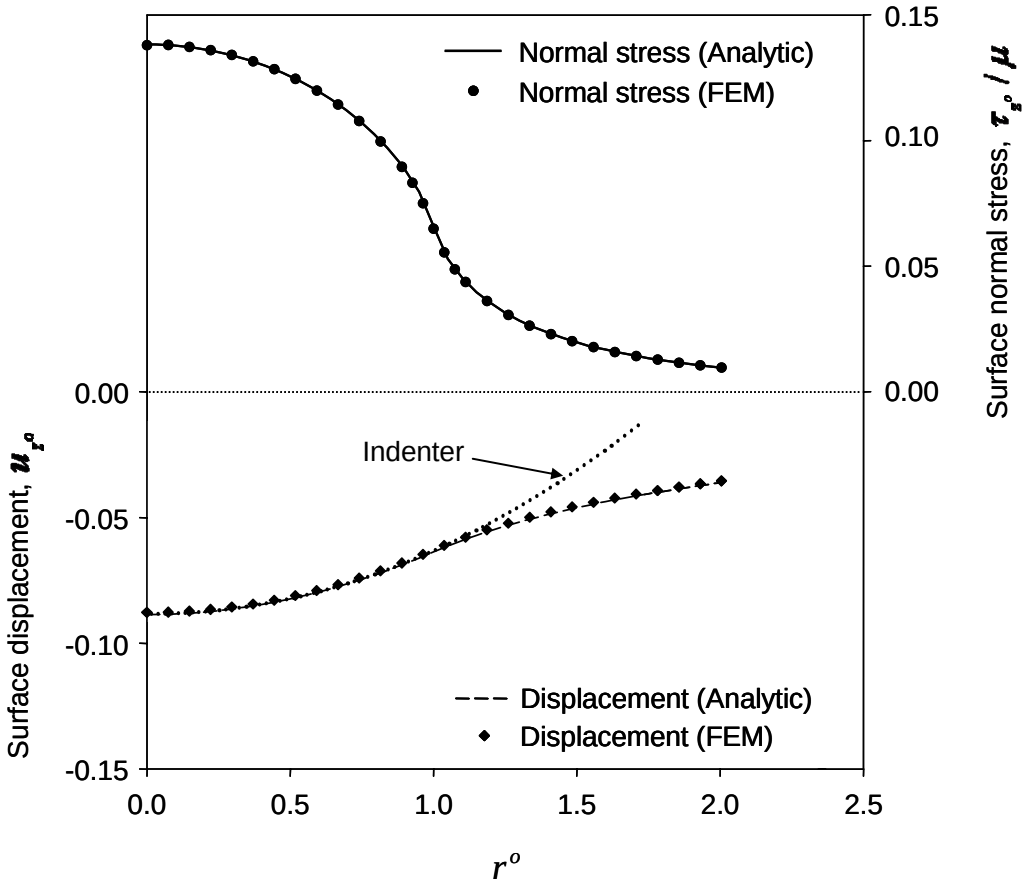

Figure 4.6 Stress distribution and displacement on the surface of elastic solid; $\nu = 0.43,\ \ a/R = 0.05,\ \ T_o(1-\nu)/\mu = 0.5\,cm$. Solid lines are from analytical solution, dots are from FE simulation. Stress is normalized by shear modulus and displacement is normalized by contact radius.

Figure 4.7b shows how the normalized (z/a) location of maximum shear stress varies as a function of a/R. As expected, in the Hertzian case ($T_o = 0$) this location is a constant. However, a decrease is shown, with increasing a/R, for all other cases with finite membrane tension. This is due to the decrease in membrane 'effect' as contact dimensions increase (see Eq. 4.19). Note that the data shown are for constant R. It is expected that whereas the attachment conditions between membrane and solid have little effect on the results in Eqs. (4.25) and (4.26) [44], under larger deformation an attached membrane could significantly affect stress distributions (see section 4.6) . Finally, in cases of physiologic visceral contact, sufficient moisture exists to provide relatively frictionless conditions. Nevertheless, our FEM models with a friction coefficient of 0.1 (not shown) suggest that within the applicable range of this model, indenter/membrane friction has little effect.

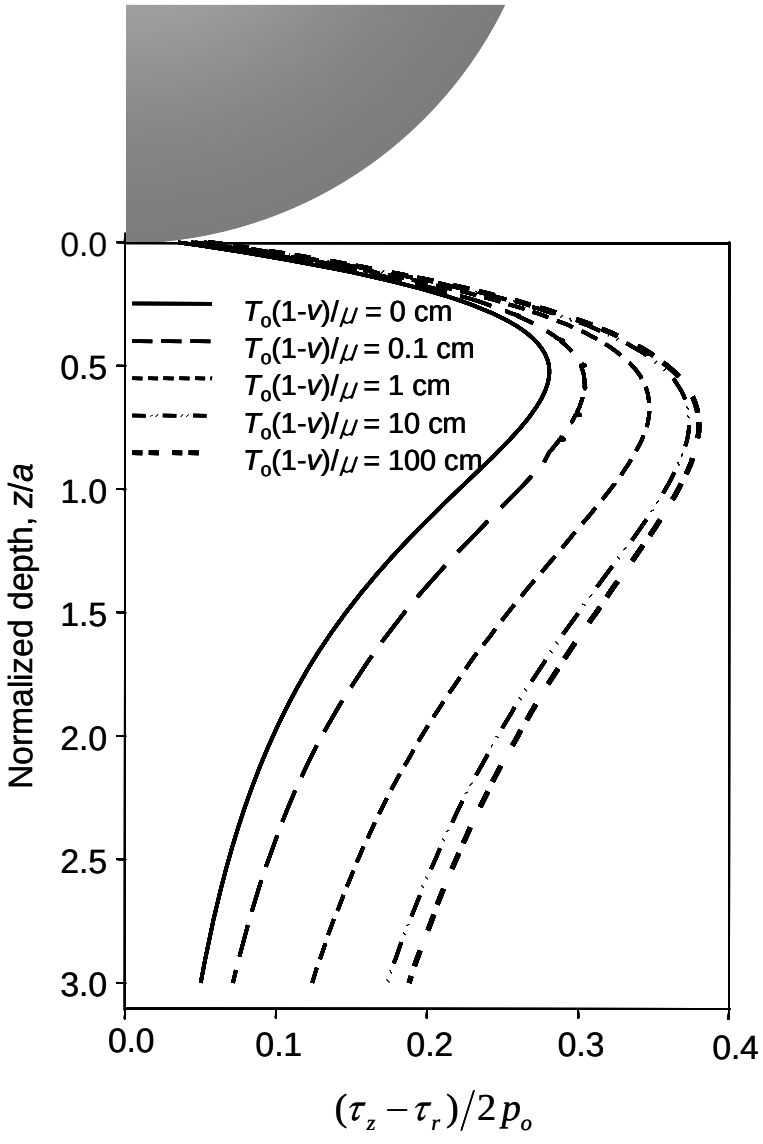
0.0
0.5
1.0
1.5
2.0
2.5
3.0
Normalized depth, z/a
$T_o(1-\nu)/\mu$ = 0 cm
$T_o(1-\nu)/\mu$ = 0.1 cm
$T_o(1-\nu)/\mu$ = 1 cm
$T_o(1-\nu)/\mu$ = 10 cm
$T_o(1-\nu)/\mu$ = 100 cm
0.0
0.1
0.2
0.3
0.4
$(\tau_z - \tau_r)/2p_o$

(a)

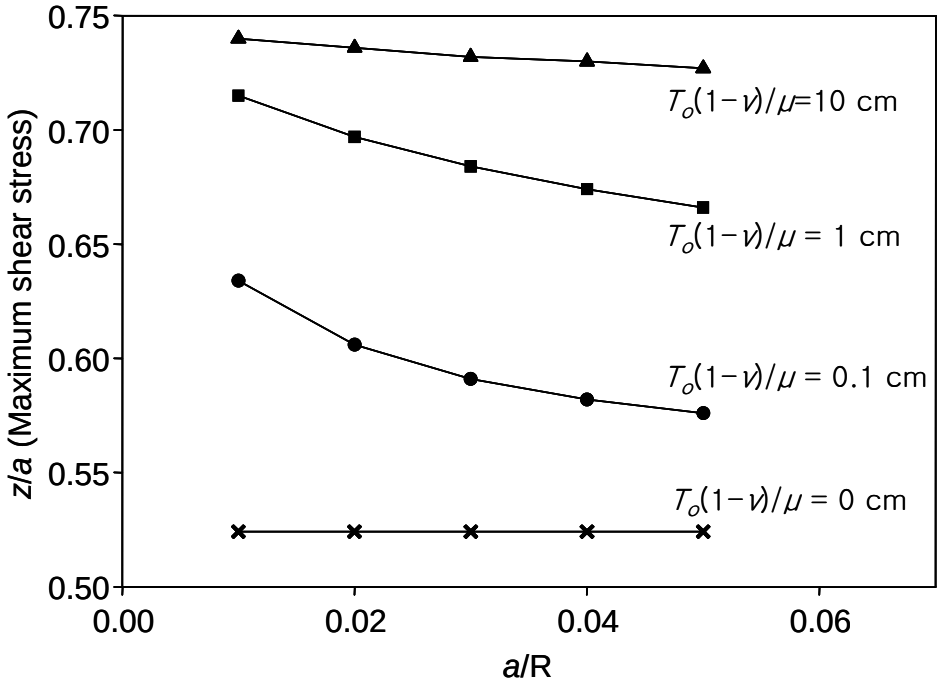

(b)

Figure 4.7 (a) Shear stress distributions along the axis of symmetry with variable membrane tension; $\nu = 0.43$, $\mu = 3.5\,kPa$. Maximum shear stress depth increases as membrane effect increases. (b) Maximum shear stress depth – contact radius curves; $\nu = 0.43$, $\mu = 3.5\,kPa$. Contrary to the case without membrane effect, the maximum depth is increasing as the tension increases and decaying from maximum as the contract radius increases.

4.6 Conclusion

In this chapter, a solution for spherical indentation of an elastic half-space covered with a tensed membrane is developed. Semi-analytical relations show good agreement with FEM models, over a range of input parameters. The modified boundary condition is proved to be valid for various combinations of modulus and membrane tension. The plot of shear stress based on current solution shows that the location of maximum shear stress deviates from the prediction of classic solution and decreases as the normalized contact radius increases. Though the attachment between the membrane and the elastic solid is the real case, the free sliding assumption shows negligible effect on the results. It is intended that this solution is appropriate for macro- or perhaps micro-indentation of biological tissues. FEM results with large depth indentation illustrates that the compressive pressure possibly induce the shrinkage of local region of lung, leading to collapse.

5. Spherical Indentation of An Elastic Bilayer

5.1 Introduction

In this chapter, the spherical indentation on an elastic layered system is considered. New perturbation solution is presented compared to FEM results. The effect of the tip geometry on the measured modulus will be discussed.

After the instrumented indentation was adopted for measurement of mechanical property, its application has been extended to the film measurement. Due to the lack of an exact solution for a film/substrate system, there have been numerous models for the relationship between the effective modulus μ_{eff} of the film/substrate system and the film/substrate moduli (μ_f and μ_s). Most of these works were based on flat-ended and sharp tip indentation aimed at application to nanoindentation.

Doerner and Nix [11] first proposed an exponential equation for the effective modulus based on their experimental data using nanoindentation. King [29] modified this equation by doing numerical analysis of flat-ended tip indentation. The above empirical equations have adjustable parameters which must be determined by experiment, or numerically.

Gao, et al.[31] derived a first order perturbation solution for the flat punch indentation problem, showing that their solution is valid up to the modulus mismatch ratio of 2. Xu and Pharr[47] later modified the perturbation solution and comparison with FEM results showed better accuracy for a wide range of modulus mismatch. The perturbation solution is attractive because it is given as a closed form and doesn't include

adjustable parameters. But its assumption on flat-ended cylindrical geometry limits the applicability for sharp or spherical tip indentation, particularly when a and t are comparable.

Different tip geometries have been considered in other investigations. Perriot and Barthel[48] used numerical integration to get effective modulus curves for sharp and spherical tips, and showed they overlap closely, but differ from those for a flat-ended cylindrical tip. Clifford and Seah[26] conducted FEM simulations with spherical tip geometry to get effective modulus curves for compliant polymer films on stiff substrates and proposed a curve-fit equation. Finally, Hsueh and Miranda[49] presented an approximate, analytically derived equation of effective modulus under spherical tip indentation, based on an extension of the Boussinesq Green's function. Using FEM simulations, they showed that their results were valid for a certain range of modulus mismatch, but most accurate for the case of a compliant film on a stiff substrate.

There is an opportunity to revisit the problem of spherical indentation of a bilayer, with particular attention to the stiff film on compliant substrate. From the above investigations it appears that inaccuracies may arise from (a) tip geometry (e.g., flat punch vs spherical) or (b) analysis method. To investigate this, here we use the first-order perturbation solution, and modify it for a spherical tip geometry. The following salient points will be made:

- A known solution for indentation of a homogeneous half-space is used to calculate the energy change due to perturbation of modulus. Specifically, we adapt Gao's solution to accommodate the stress/displacement distribution under a spherical tip.
- FEM simulation is conducted to verify the new solution. FEM results for a

spherical tip are compared to those for a flat-ended cylindrical tip for the examination of the effect of tip geometry on effective modulus measurement.

- Improved agreement is shown between the new approach and FEM/numerical approaches, particularly in the case of a stiff film on a compliant substrate.

5.2 Elastic solution for spherical indentation of an elastic half space

The problem of spherical contact was first studied by Hertz [1]. He solved integral equation and presented the contact stresses. The stress beneath the surface was first analyzed by Huber [50]. Fuch [51] settled the lines of principal stress by carrying out a laborious process of arithmetical integration. Later, Morton and Close [52] calculated the stresses developed in the half-space on which a spherical ball is pressed. None of the above works presented an applicable solution with explicit formulation. The fully derived formulation of stress field under spherical contact was given by Hamilton and Goodman [53], but their formulation was in an implicit form involving imaginary parts. Hamilton [54] extracted the stresses as a series of algebraic formulae based on Hamilton and Goodman's result.

The stress field for the frictionless spherical contact problem given by Hamilton is as follows;

$$\tau_{rr} = \frac{3P}{2\pi a^3}\left[z(1+\nu)\phi + \frac{1}{r^2}\left\{ aMz\nu - Nr^2 - \frac{aMr^2 z}{S} + \frac{(1-2\nu)}{3}(a^3 + 2AN + NS) - (1-\nu)Nz^2 \right\}\right] \tag{5.1}$$

$$\tau_{\theta\theta} = \frac{3P}{2\pi a^3}\left[z(1+\nu)\phi - \frac{1}{r^2}\left\{ aMz\nu + 2Nr^2\nu + \frac{(1-2\nu)}{3}(a^3 + 2AN + NS) - (1-\nu)Nz^2 \right\}\right] \tag{5.2}$$

$$\tau_{zz} = \frac{3P}{2\pi a^3}\left[-N + \frac{aMz}{S}\right], \tag{5.3}$$

$$\tau_{rz} = -\frac{3P}{2\pi a^3}\left[z\left\{\frac{Nr}{S} - \frac{Hrz}{G^2 + H^2}\right\}\right], \tag{5.4}$$

where

$A = r^2 + z^2 - a^2$; $S = (A^2 + 4z^2a^2)^{1/2}$

and

$$M = \left(\frac{S + A}{2}\right)^{1/2}; N = \left(\frac{S - A}{2}\right)^{1/2}; \phi = \tan^{-1}\left(\frac{a}{M}\right)$$

and

$G = M^2 - N^2 + zM - aN$; $H = 2MN + aM + zN$.

The strain field is deduced from Hooke's law to give

$$\varepsilon_r = \frac{-P}{4\pi a^3 r^2 S\mu}\left[3Sz(Nz + r^2\phi)(1-\nu) - S(a^3 + 2AN - 3Nr^2 + SN)(1-2\nu) + 3aM(r^2 - S\nu)\right] \tag{5.5}$$

$$\varepsilon_z = \frac{3P}{4\pi a^3 S\mu}\left[z(aM - 2S\nu\phi) - NS(1-2\nu)\right], \tag{5.6}$$

$$\varepsilon_\theta = \frac{P}{4\pi a^3 r^2 \mu}\left[(3Nz^2 + 3r^2 z\phi)(1-\nu) - (NS + a^3 + 2AN)(1-2\nu) - 3aMz\nu\right], \tag{5.7}$$

Similarly, the displacement field is given as

$$u_r = \frac{P}{4\pi a^3 r\mu}\left[(3Nz^2 + 3r^2 z\phi)(1-\nu) - (NS + a^3 + 2AN)(1-2\nu) - 3aMz\nu\right], \tag{5.8}$$

$$u_z = \frac{3P}{16\pi a^3 \mu}\left[\pi(2a^2 - r^2)(1-\nu) + 4\int_0^z\left(\frac{z(aM - 2S\nu\phi) - NS(1-2\nu)}{S}\right)dz\right] \qquad r \le a\,, \tag{5.9}$$

$$u_z = \frac{3P}{8\pi a^3 \mu}\left[\left(ar\sqrt{1-\frac{a^2}{r^2}} + (2a^2 - r^2)\sin^{-1}\left(\frac{a}{r}\right)\right)(1-\nu) + 2\int_0^z \left(\frac{z(aM - 2S\nu\phi) - NS(1-2\nu)}{S}\right)dz\right]$$

$$r > a, \qquad (5.10)$$

In the next section, the stress, displacement and strain field (Eqs. 5.1-10) will be used to calculate the strain energy due to a moduli perturbation.

5.3 Perturbation analysis

Figure 5.1 shows a schematic of the problem to be addressed, namely the indentation of a film/substrate system with a rigid spherical tip of radius R. Cylindrical coordinates r, θ, z are used and the system is axisymmetric about the z-axis ($r = 0$). The contact surface and the film/substrate interface are located at $z = 0$ and $z = t$, respectively. An applied load P results in tip displacement h and the contact radius a. Both film and substrate are isotropic linear elastic solids, with shear modulus and Poisson's ratio μ_f, ν_f and μ_s, ν_s, respectively. In perturbation analysis, the film/substrate system is treated as a homogeneous material with (initially) properties of the substrate that undergoes a phase transformation to assume film properties in the region $0 < z < t$. During the transformation, the load P is fixed and the displacement h is allowed to change to $h + \delta h$. The force-displacement relation for spherical indentation of an elastic material, is described by Hertzian relation[2] as

$$P = \frac{8\sqrt{R}h^{3/2}\mu}{3(1-\nu)} \qquad (5.11)$$

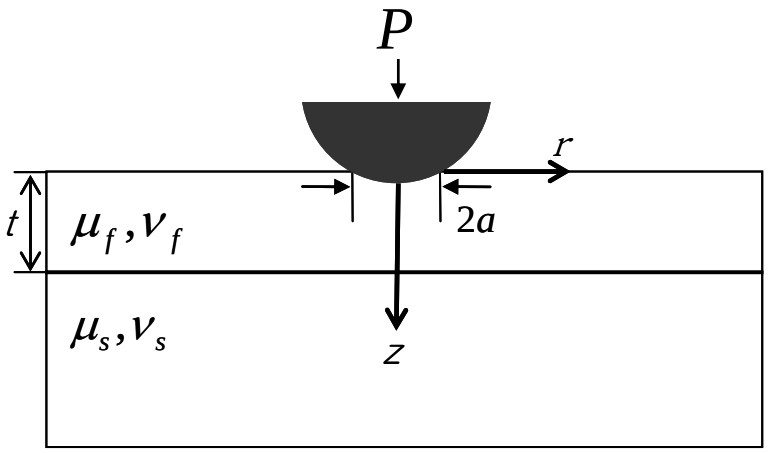

Figure 5.1 Schematic of spherical indentation on film/substrate system

Equation (5.11) contains a single value for shear modulus and Poisson's ratio, but a composite value is used to represent the film/substrate system [26, 49, 55]. Upon the phase transformation, the extra work done by the force P due to the displacement change ∂h is thus calculated as [56]

$$W = \int P\partial h = \int \frac{8\sqrt{R}h^{3/2}\mu}{3(1-\nu)}\partial h = \frac{2}{5}Ph,$$

$$\partial W = \frac{2}{5}P\partial h \tag{5.12}$$

The additional work is equal to the strain energy change due to moduli variation in the body, and the energy conservation equation can be written as

$$\frac{2}{5}P\delta h = -\frac{1}{2}\int_{V_f} \delta c_{ijkl} u^o_{i,j} u^o_{k,l} dV \tag{5.13}$$

where δc_{ijkl} is the change of moduli from substrate material to film material and u^o_i is the known displacement field for the homogeneous substrate material. The right term of Eq. (5.13) is the energy variation due to a moduli transformation, and can be rearranged (following Gao, et al.[31]) as

$$\frac{2}{5}P\delta h = -\frac{1}{2}e\lambda_s \int_{V_f} \varepsilon^o_{jj}\varepsilon^o_{kk} dV - \frac{1}{2}\frac{\mu_f - \mu_s}{\mu_s}\int_{A_f} \tau^o_{ij} n^o_i u^o_j dA, \tag{5.14}$$

where λ_s is the Lame constant of the substrate,

$$e = \frac{\mu_f}{\mu_s}\cdot\frac{(\nu_f - \nu_s)}{\nu_s(1-2\nu_f)}, \tag{5.15}$$

and τ^o and ε^o are the known stress and strain field for the homogeneous substrate material. The terms V_f and A_f in Eq. (5.14) indicate the domain volume and the surrounding surface domain of the film region, respectively. The surface domain consists of two planes: $z = 0$ and $z = t$. The surface stress and displacement solutions

for spherical indentation of an elastic homogeneous material are known[2], and are

$$u_z = \frac{1-\nu}{\mu}\frac{\pi p_o}{8a}(2a^2 - r^2) \quad r \le a\,, \tag{5.16}$$

$$\tau_{zz} = p_o(1 - r^2/a^2)^{1/2} \qquad r \le a\,, \tag{5.17}$$

where

$$p_o = \frac{4h\mu}{\pi a(1-\nu)} = \frac{3P}{2\pi a^2}. \tag{5.18}$$

Using Eqs. (5.16-18), the area integral on the surface in Eq. (5.14) reduces to $4/5\,Ph$. Substitution and rearrangement of Eq. (5.14) leads to the following expression for $\partial h / h$

$$\frac{\delta h}{h} = -\frac{5}{4}\frac{e\lambda_s}{Ph}\int_{V_f}\varepsilon^o_{jj}\varepsilon^o_{kk}dV - \frac{\mu_f - \mu_s}{\mu_s}\left[1 + \frac{5}{2}\frac{\pi}{Ph}\int_0^\infty(\tau^o_{zz}u^o_z + \tau^o_{rz}u^o_r)_{z=t}\,rdr\right] \tag{5.19}$$

The original displacement h is calculated from the Hertz relation[2] such as

$$h = \frac{3P(1-\nu)}{8a\mu} \tag{5.20}$$

Since the total displacement h_t is given as $\delta h + h$,

$$h_t(a/t) = \frac{3P(1-\nu_s)}{8a\mu_s}\left[1 - \frac{\nu_f - \nu_s}{1-\nu_s}I_1(a/t) - \frac{\mu_f - \mu_s}{\mu_s}I_o(a/t)\right] \tag{5.21}$$

where

$$I_o(a/t) = 1 + \frac{5}{2}\frac{\pi}{Ph}\int_0^\infty(\tau^o_{zz}u^o_z + \tau^o_{rz}u^o_r)_{z=t}\,rdr\,, \tag{5.22}$$

$$I_1(a/t) = \frac{5}{4}\frac{\mu_s(1-2\nu_f)(1-\nu_s)}{\mu_f(1-2\nu_s)(\nu_f - \nu_s)}\frac{e\lambda_s}{Ph}\int_{V_f}\varepsilon^o_{jj}\varepsilon^o_{kk}dV\,. \tag{5.23}$$

Equation (5.21) is thus the perturbation equation for spherical indentation. The terms I_o and I_1 are weighting functions representing modulus difference and Poisson's ratio difference, respectively. For the flat punch, Neuber's potential [57] was used to

calculate I_o and I_1. Here, the elastic solutions for the spherical punch problem given by Hamilton [53, 54] are used to obtain new I_o and I_1.

Substituting Eqs. (5.1-10) into Eqs. (5.22) and (5.23) gives closed-form integral equations for I_o and I_1 for spherical indentation:

$$
\begin{aligned}
I_o &= 1+\frac{5}{4\pi a^5(1-\nu)} \\
&\times\left\{\int_0^a\left[\frac{3}{2}\left(-N'+\frac{aM't}{S'}\right)\left(\pi(2a^2-r^2)(1-\nu)+4\int_0^t\left(\frac{z(aM-2S\nu\phi)-NS(1-2\nu)}{S}\right)dz\right)\right]rdr\right. \\
&+\int_a^\infty\left[3\left(-N'+\frac{aM't}{S'}\right)\left(\left(ar\sqrt{1-\frac{a^2}{r^2}}+(2a^2-r^2)Sin^{-1}\left(\frac{a}{r}\right)\right)(1-\nu)\right.\right. \\
&\left.+2\int_0^t\left(\frac{z(aM-2S\nu\phi)-NS(1-2\nu)}{S}\right)dz\right]rdr \\
&\left.+\int_0^\infty\left[2t\left(\frac{N'r}{S'}-\frac{H'rt}{G'^2+H'^2}\right)\left((3N't^2+3r^2t\phi)(1-\nu)-(N'S'+a^3+2A'N')(1-2\nu)-3aM't\nu\right)\right]rdr\right\}
\end{aligned}
\tag{5.24}
$$

$$
I_1=\frac{30}{\pi}\int_0^t\int_0^\infty(N-z\phi)^2\,rdrdz\,, \tag{5.25}
$$

where A', S', M', N', G', H' are variables in Eqs. (5.1-10) at $z=t$. Equations (5.24) and (5.25) represent weighting functions for the modulus and Poisson's ratio effects, respectively, taking into account a spherical indenter.

It is important to note that the perturbation analysis presented here is based on the assumption that the contact radius a remains constant during transformation. However, with a spherical tip of constant radius R this is not the case, as a change in effective modulus would indeed change h, giving a concomitant change in a. To avoid this complication, we allow *tip* radius R to vary during transformation but constrain a to be constant. This is permitted using Hertzian analysis, as the surface pressure boundary condition is described with load P and contact radius a in spherical

indentation as in Figure 5.2. Elastic solutions for stress and displacement (Eqs. 5.1-10) depend *only* on this pressure boundary condition. If the two cases in Figures 5.2 a and b have the same boundary condition, the relative strain energy difference between the two states can be predicted by the moduli perturbation equation as expressed in the right term of Eq. (5.13). On the other hand, the left term in Eq. (5.13) gives the relative elastic stored energy change between two states in Figures 5.2 a and b. By considering a different radius of the sphere, Eq. (5.13) is applicable to the layered contact problem.

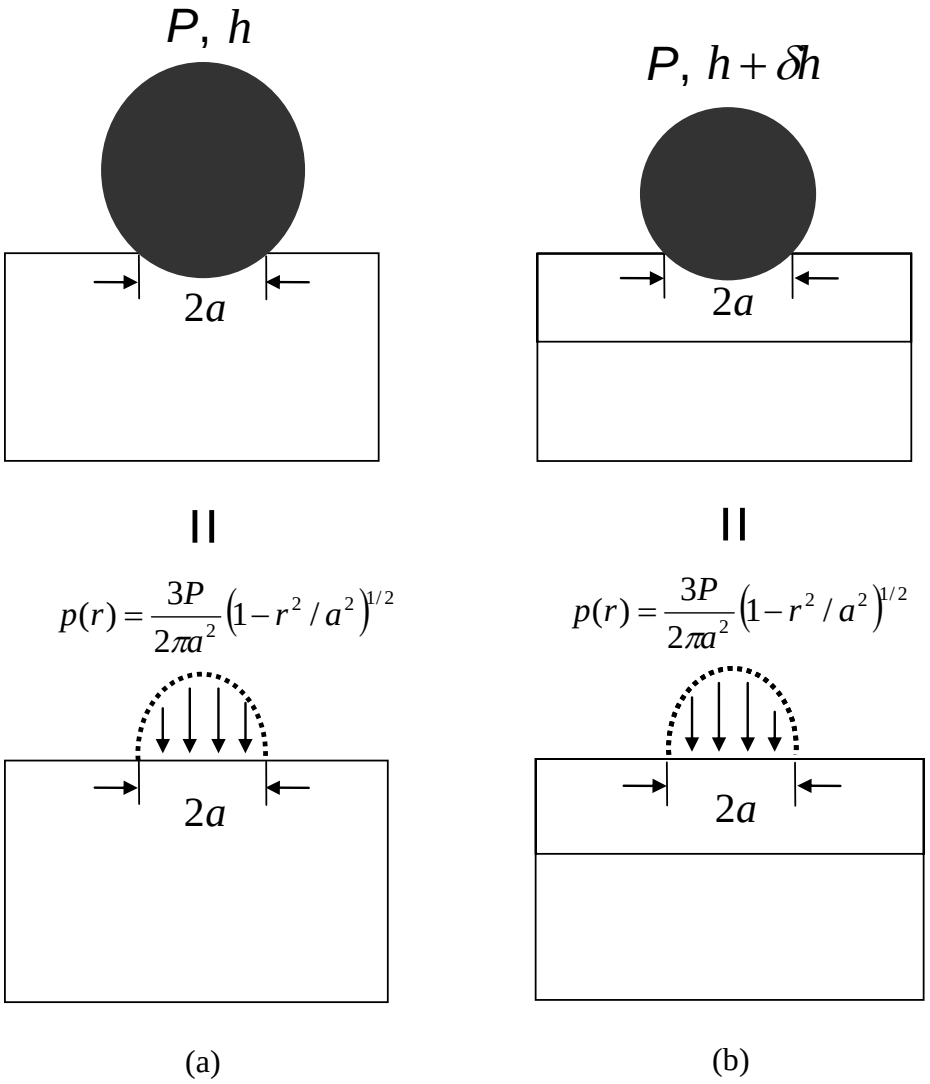

Figure 5.2 Pressure boundary condition with different ball size (a) before and (b) after phase transformation.

5.4 Effective compliance

The moduli perturbation can also be accomplished via transformation of the substrate ($t < z < \infty$.) Thus, another perturbation equation is given in similar form to Eq. (5.21) when the transformation occurs in the substrate region,

$$h_t(a/t) = \frac{3P(1-\nu_f)}{8a\mu_f}\left[1-\frac{\nu_s-\nu_f}{1-\nu_f}(1-I_1)-\frac{\mu_s-\mu_f}{\mu_f}(1-I_o)\right]. \qquad (5.26)$$

Noting that Eqs. (5.21) and (5.26) must agree with each other, Gao et al. [31] suggested the two equations be combined to give the unified form for effective compliance as

$$\left[\frac{1-\nu}{\mu}\right]_{eff} = \frac{1-\left[\nu_f I_1+\nu_s(1-I_1)\right]}{\mu_f I_o+\mu_s(1-I_o)} \qquad (5.27)$$

It is clear that although Eq. (5.27) gives correct values at limiting cases of $a/t \to 0$ (complete sampling of film) and $a/t \to \infty$ (complete sampling of substrate), its limit as $\mu_s \to \infty$ is not correct. In addition, 7% error was shown between Eq. (5.27) and flat punch FEM models in the range of $0.5 < \mu_f/\mu_s < 2$. Xu and Pharr [47] modified Eq. (5.27) to give the correct limit as $\mu_s \to \infty$

$$\left[\frac{1-\nu}{\mu}\right]_{eff} = \left[1-\nu_s+(\nu_s-\nu_f)I_1\right]\left[\frac{(1-I_o)}{\mu_s}+\frac{I_o}{\mu_f}\right] \qquad (5.28)$$

Using FEM simulations, they showed that Eq. (5.28) gives better accuracy for a wider range of $0.1 \le \mu_f/\mu_s \le 10$. For comparison of modulus extraction methods, Eqs. (5.27) and (5.28) may be used to plot curves of effective modulus vs a/t (see later Figures). For further illustration, a normalized displacement may be defined and compared across methods[49]. This term, denoted as h_t/h_f compares tip displacement under identical

loading conditions, between a composite material and a homogeneous material having film properties. The displacement for the composite material and the film only material can be given by rearranging Eq. (5.11) such as

$$h_t = \left[\frac{3P}{8\sqrt{R}} \left(\frac{(1-\nu)}{\mu} \right)_{eff} \right]^{2/3} \tag{5.29}$$

$$h_f = \left[\frac{3P}{8\sqrt{R}} \left(\frac{(1-\nu)}{\mu} \right)_{f} \right]^{2/3} \tag{5.30}$$

where $\left((1-\nu)/\mu\right)_f$ is the compliance of the film, h_t is the displacement for the film/substrate system and h_f is the displacement for the film only material under the same load and geometry. Comparing Eqs. (5.29) and (5.30), the normalized displacement can be given as

$$h_t / h_f = \left[\left(\frac{(1-\nu)}{\mu} \right)_{f} \Big/ \left(\frac{(1-\nu)}{\mu} \right)_{eff} \right]^{2/3} \tag{5.31}$$

5.5 Results and discussion

The new weighting functions I_o and I_1 for spherical punch (Eqs. 5.24, 5.25) are displayed in Figure 5.3 compared to those for flat punch[31]. The new functions for spherical punch have a similar shape, but are not equivalent to those for flat punch. The curves for the spherical case have inflection points that occur for larger contact radius than the flat punch. Thus, the flat punch case underestimates the values of I_o and I_1 for ratios of contact radius to layer thickness (a/t) ranging from 0.02 to 2; and

overestimates the values of I_o and I_1 for a/t ranging from 2 to 100. Near the equivalence points of the spherical and flat punch cases at $a/t = 2$ for I_o, and $a/t = 5$ for I_1, there is similarity in the results. Both weighting functions go to unity and zero as $a/t \to 0$ and $a/t \to \infty$, respectively. Figure 5.4 shows the evolution of effective modulus with varying a/t. Consider the film-substrate system described in this work. With input values of μ_f and μ_s, μ_{eff} is the modulus that would be obtained in an experiment. For a spherical indenter of radius R, this value would be calculated using Eq. (5.11). For a flat punch, this would be calculated using the following equation [41]:

$$P = \frac{4ah\mu}{(1-\nu)} \tag{5.32}$$

In Figure 5.4a, Eq. (5.27) is plotted using I_o derived in this work (Eq. 5.24), and I_o for a flat punch. Poisson's ratio for both a film and a substrate is set to 0.3 so that I_1 is not considered here. The Figure shows that using Eq. (5.27) one obtains a single curve the position of which is independent of modulus ratio. In Figure 5.4b, Eq. (5.28) is plotted using I_o for both the current work and flat punch, and the curves correctly shift as the modulus ratio varies. Note that although the curves have similar shapes there are large deviations between values of effective modulus for flat and spherical tips. This deviation is highest when modulus ratio μ_f / μ_s becomes very small.

To check the correctness of the approach, results from Eqs. (5.24), (5.25) and (5.28) were compared with finite element simulations using the commercial code ABAQUS[36]. The spherical indentation on layered system was modeled as described in section 3.2.2. Film thickness t was varied to determine effective modulus in the range $0.02 \le a/t \le 100$.

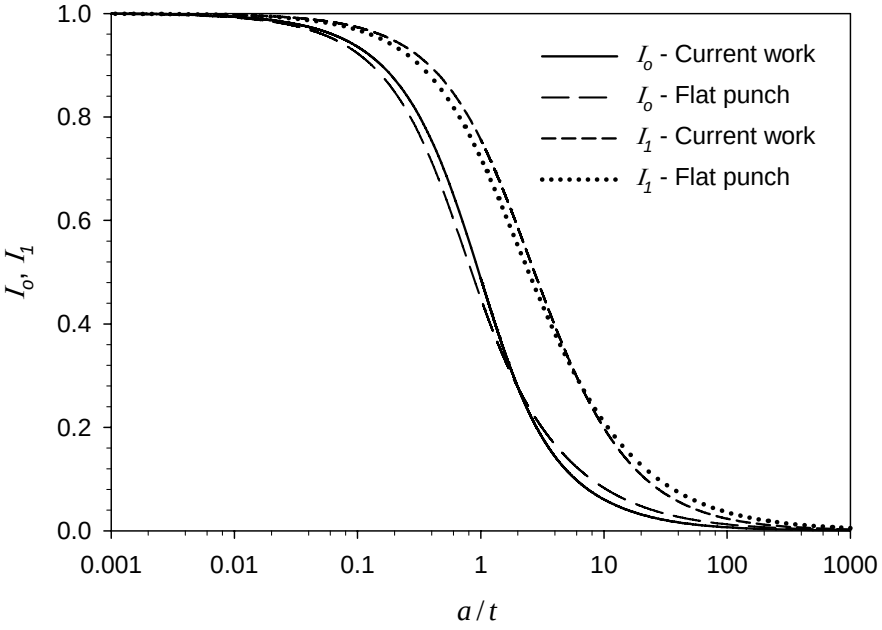

Figure 5.3 I_o and I_1 curves for spherical and flat punches.

For comparison, flat punch indentation was also simulated with variable thickness of the film. Poison's ratio was fixed at 0.3 for the film and the substrate. The effective modulus was obtained with Eq. (5.11) and Eq. (5.32) for spherical and flat punch, respectively. Figure 5.5 displays the FEM results for two different indenter shapes compared to the current solutions (using Eq. 5.28) and Gao's analytical model for a flat punch [31]. Figure 5.5(a-b) illustrates the cases of a stiff film on a compliant substrate, and Figure 5.5(c-d) represents the cases of a compliant film on a stiff substrate. The normalization in Figure 5.5 indicates how the effective modulus changes between the film modulus and substrate modulus. A normalized value approaching, 0 and 1 means the effective modulus converges to the film modulus and substrate modulus, respectively.

Examination of FEM results shows that the relation between μ_{eff}, μ_f and μ_s over a range of a/t differs significantly between a flat punch and a spherical tip. The difference is maximum in cases where a and t are comparable, and $\mu_f > \mu_s$. The two curves converge when a/t goes to zero or infinity. This is perhaps not surprising. In all cases, Gao's flat punch solution with the modified equation (Eq. 5.28) underestimates the modulus for both stiff and compliant film cases. That is to say, the predicted μ_{eff} for a given set of μ_f, μ_s and a/t is lower than that extracted from the FEM models. The current solution for spherical punch (with Eq. 5.28) gives good agreement with FEM for stiff films, but underestimates for compliant films. Figure 5.6 illustrates the normalized displacement (Eq. 5.31) curves comparing the current work with FEM results and Hsueh's model[49]. Note that Hsueh's model gives a very similar result to the current solution when the modulus mismatch is small for the case of stiff films, but when the mismatch increases, it shows larger deviation.

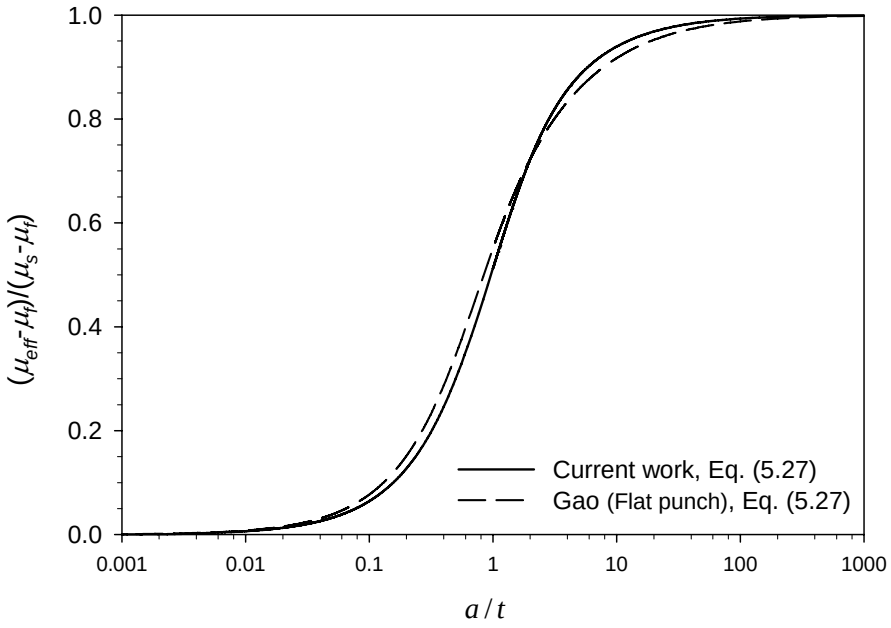

(a)

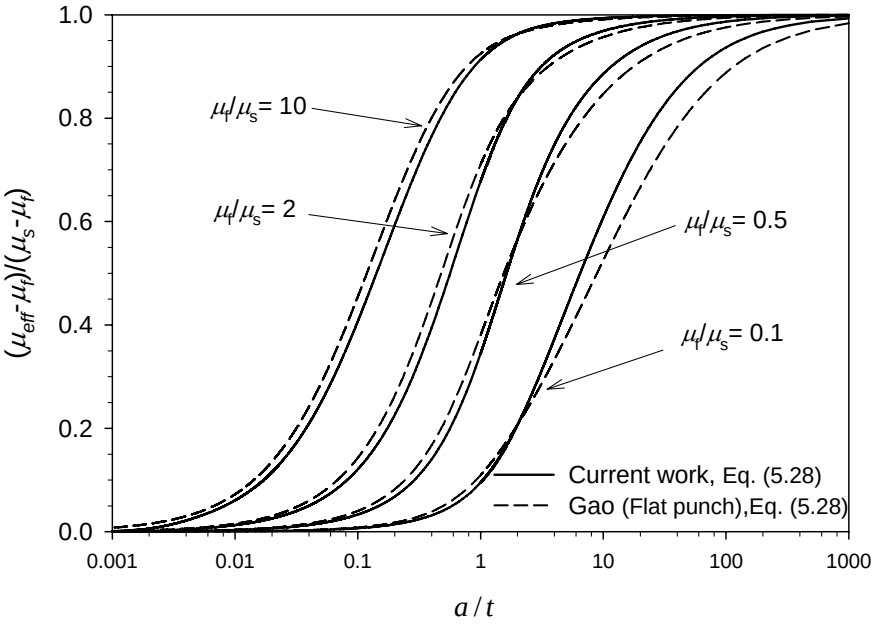

(b)

Figure 5.4 Evolution of the effective modulus μ_{eff} with a/t for spherical punch (solid line) and flat punch (dashed line). (a) Plots of Eq. (5.27) and (b) Eq. (5.28). Values of ν_f and ν_s were fixed at 0.3.

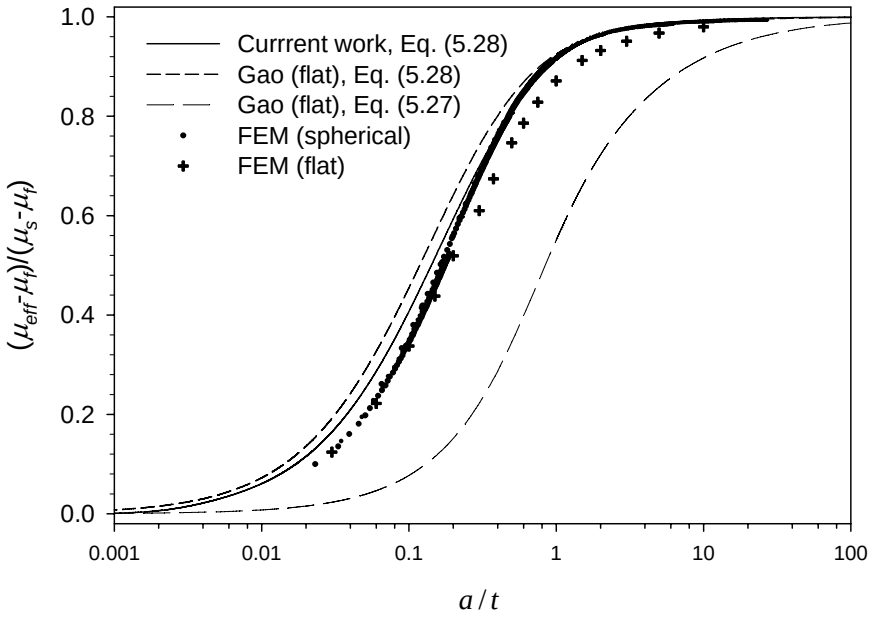
Currrent work, Eq. (5.28)
Gao (flat), Eq. (5.28)
Gao (flat), Eq. (5.27)
FEM (spherical)
FEM (flat)
$(\mu_{eff}-\mu_f)/(\mu_s-\mu_f)$
a/t
1.0
0.8
0.6
0.4
0.2
0.0
0.001
0.01
0.1
1
10
100

(a)

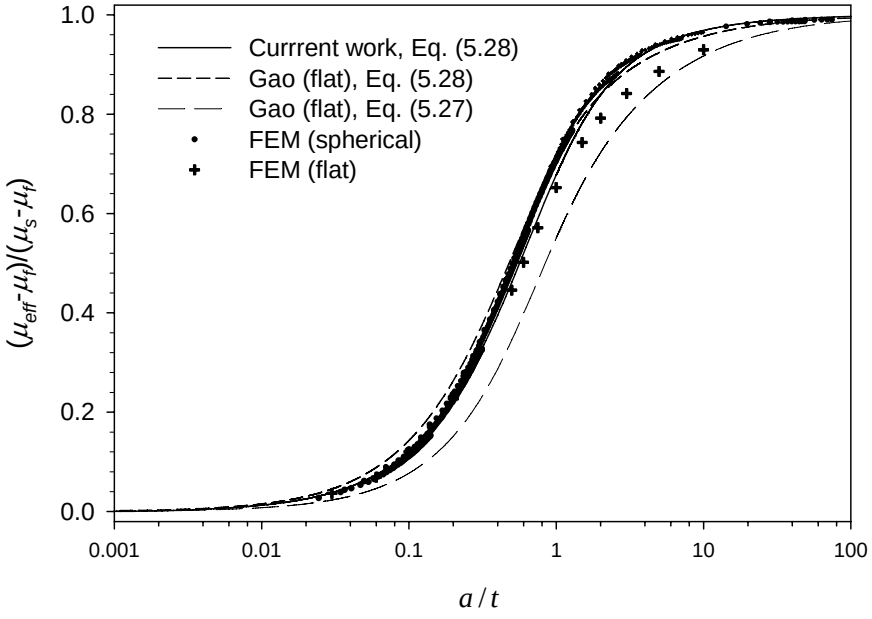
Currrent work, Eq. (5.28)
Gao (flat), Eq. (5.28)
Gao (flat), Eq. (5.27)
FEM (spherical)
FEM (flat)
$(\mu_{eff}-\mu_f)/(\mu_s-\mu_f)$
a/t
1.0
0.8
0.6
0.4
0.2
0.0
0.001
0.01
0.1
1
10
100

(b)

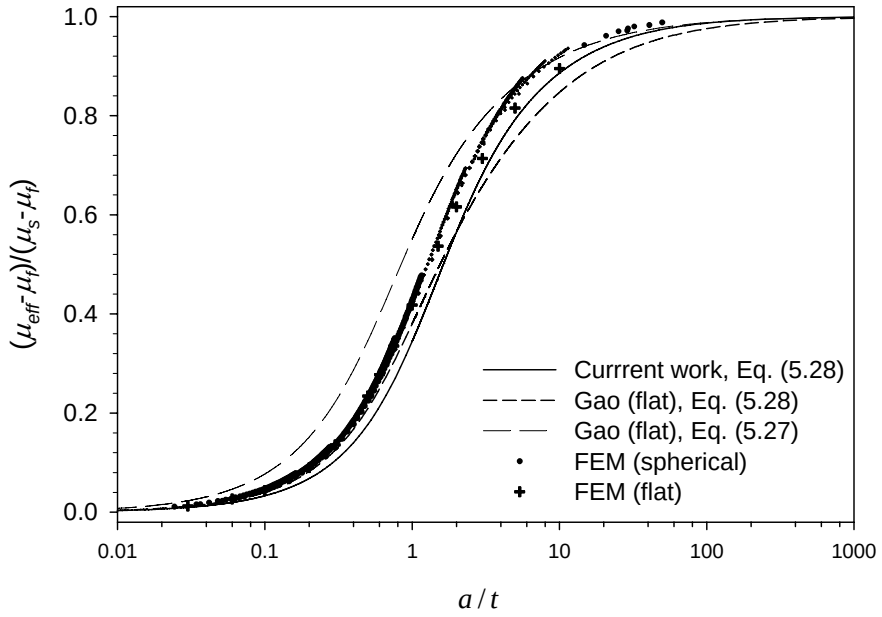

(c)

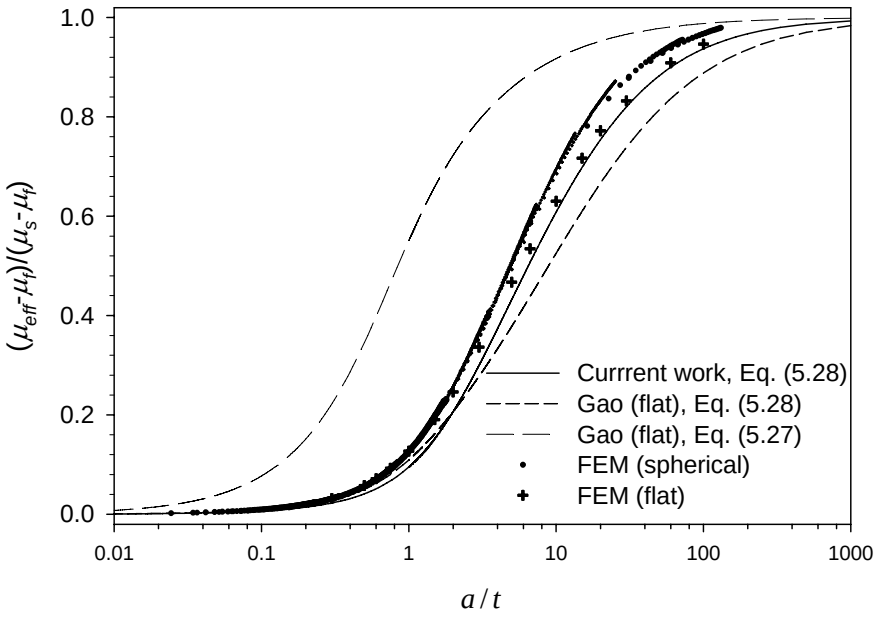

(d)

Figure 5.5 Comparison of FEM results to the current work (using Eq. 5.28) and Gao's solution for stiff films (a) [$\mu_f / \mu_s = 10$], (b) [$\mu_f / \mu_s = 2$] and compliant films (c) [$\mu_f / \mu_s = 0.5$], (d) [$\mu_f / \mu_s = 0.1$].

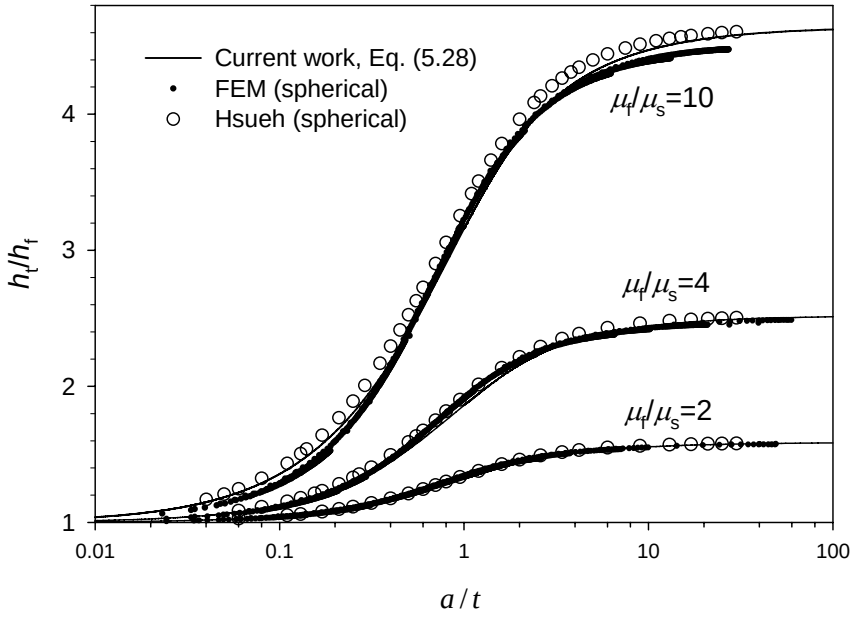

(a)

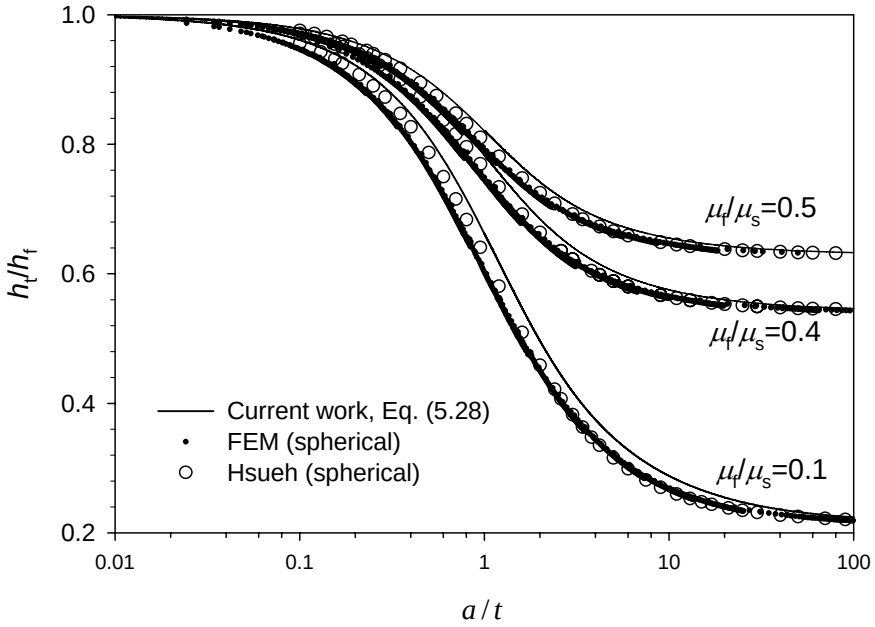

(b)

Figure 5.6 Normalized displacement, h_t / h_f curves for the current work with comparison to FEM results and Hsueh's model: (a) $\mu_f / \mu_s = 2$,4 and 10, and (b) $\mu_f / \mu_s = 0.1$, 0.4 and 0.5.

For $\mu_f / \mu_s = 10$, both Hsueh's and the current solution deviate from the FEM results when $a/t \to \infty$. Hsueh et. al attributed this discrepancy to flexural stresses in the film. The current solution underestimates the modulus in the case of compliant films. We find this acceptable, as Hsueh's solution is sufficiently accurate in those cases. Finally, it is interesting to note that in the case of stiff films, the current solution appears most accurate when a and t are comparable.

In considering the accuracy of Gao's original approach, one must account for errors arising from (a) the method of analysis and (b) the indenter shape approximation. When Gao, et al first derived a solution for the flat punch, they mentioned that the solution is correct with 7% error within $0.5 \le \mu_f / \mu_s \le 2$, when compared with FEM for the same shape. Subsequently, Xu and Pharr modified Gao's solution and showed that its accuracy increased in a wider range $0.1 \le \mu_f / \mu_s \le 10$. However, Figure 5.5 shows that their modified solution is still off from the FEM results for all cases. Addressing the indenter shape, error could result from using Neuber's potential for an external crack to calculate the strain energy for the flat punch geometry. The stress singularity of flat punch at the corner may lead to differences with the FEM simulation.

Our current solution is based on the same perturbation approach, but we are using a more practical geometry, spherical punch, with a non-singular stress field. Figure 5.5 shows that the perturbation analysis, with a correct and readily comparable geometry, gives very accurate results, in particular for the case of a stiff film on a compliant substrate, and where a and t are comparable. This shows the remarkable applicability of the perturbation approach in this case. In the compliant film case, accuracy is less, even with the correct geometry.

5.6 Conclusion

A new analytic solution for spherical indentation of a linear elastic film/substrate bilayer is presented based on the perturbation approach previously used by Gao et al [31]. The new weighting functions (I_o, I_1) have similar shapes to those for flat punch, but deviate over most of the contact dimension range. FEM results confirm that the previous flat punch assumption gives significant error when a spherical punch is used to measure the effective modulus. The new perturbation solution gives good agreement with FEM results for stiff layers on substrates, relevant for a number of engineering systems.

6. Summary and Suggestions for Future Work

This thesis contained an examination of surface layer effects in spherical indentation of solids by recourse to an analytical approach. FEM simulation was extensively used to analyze the problems and validate the derived solutions. Errors and comparison to current and past work were discussed. Summary and suggestions for future work are as follows.

6.1 Spherical indentation of a membrane on an elastic half-space

The effect of a surface membrane on the indentation measurement of an elastic solid was studied, based on the classical elastic foundation. The membrane was implemented into the indentation problem as a *surface tension* on the elastic half-space, and for which resisting pressure is curvature-dependent. Fitting parameters were devised to predict the deviation of pressure distribution from the ideal elastic case, with the use of FEM simulation. The semi-analytic solution was universal; it was proven to be applicable for all combinations of elastic material properties and geometry, by comparison to FEM results. The current work allows evaluation of the membrane tension and the elastic modulus separately with single tip indentation, from biomaterials such as viscera or skin. Perhaps more interesting is, beyond property measurement, the stress distribution below the surface can now be predicted, which is applicable to the analysis of the onset of

plasticity for physiologic study.

In the further study, the effect of viscoelasticity should be considered. Comparison of current solution to FEM simulation with viscoelastic behavior may give the range of error, coming from elastic material assumption. Also, the current solution can be modified to include an effectively time-dependent modulus. However, currently it is thought that numerical methods would be necessary to evaluate the integral terms with time history of modulus.

6.2 Spherical indentation of an elastic bilayer

The indentation measurement on film/substrate system was studied with a perturbation approach. The energy change assuming phase transformation between a film and a substrate was calculated using the homogeneous solution for spherical indentation. Interaction between a film and a substrate was approximated by combining two perturbation equations. The perturbation solution was validated for the spherical indentation problem, especially with a system of a stiff film on a soft substrate, by comparison to FEM results. Careful investigation using FEM showed that the previous flat punch assumption gives noticeable error when a sphere is used for indentation measurement of film/substrate system, and that error is greatly reduced using the current analysis. The current work is applicable for engineering hard films such as protective films and insulating films. This could include thick tribological coatings, or DLC thin films. Experiments can now be designed such that indentation strain a/R is constrained to be low, with no limitations on the a/R ratio. This is useful as spherical indentation

with low a/R provides the ONLY true elastic analysis of these systems (flat punches have singularity at the corners, and sharp tips can only be used for elastic analysis after unloading.)

Previous models and current solution present the variation of effective modulus depending on the contact size. For the classical problem, the contact size a can be deduced from the known relation between a and depth h. For the bilayer indentation problem, this is not known *a priori* and depends on the modulus mismatch ratio. In the future work, a-h relation can be studied further using FEM simulation. Curve fitting equation for this relation would be useful for the analysis of effective modulus from indentation experiment.

References

1. H. Hertz: "Ueber die beruehrung fester elastische Koerper (On the contact of elastic solids)." Journal fur die reine und angewandte Mathematik. **92,** 156 (1882).

2. K. L. Johnson: Contact mechanics. (Cambridge University Press, New York, 1985).

3. E. H. Yoffe: Modified Hertz theory for spherical indentation. Philosophical Magazine A - Physics of Condensed Matter Structure Defects and Mechanical Properties. **50,** 813 (1984).

4. A. Gouldstone, H. J. Koh, K. Y. Zeng, A. E. Giannakopoulos and S. Suresh: Discrete and continuous deformation during nanoindentation of thin films. Acta Materialia. **48,** 2277 (2000).

5. A. M. Minor, S. A. S. Asif, Z. W. Shan, E. A. Stach, E. Cyrankowski, T. J. Wyrobek and O. L. Warren: A new view of the onset of plasticity during the nanoindentation of aluminium. Nature Materials. **5,** 697 (2006).

6. X. Chen, J. W. Hutchinson and A. G. Evans: The mechanics of indentation induced lateral cracking. Journal of the American Ceramic Society. **88,** 1233 (2005).

7. Y. P. Cao and H. Lu: A new method to extract the plastic properties of metal materials from an instrumented spherical indentation loading curve. Acta Materialia. **52,** 4023 (2004).

8. M. H. Zhao, N. Ogasawara, N. Chiba and X. Chen: A new approach to measure the elastic-plastic properties of bulk materials using spherical indentation. Acta Materialia. **54,** 23 (2006).

9. D. Tabor: A simple theory of static and dynamic hardness. Proceedings of the Royal Society of London. Series A - Mathematical and Physical Sciences. **192,** 247 (1948).

10. S. I. Bulychev, V. P. Alekhin, M. K. Shorshorov, A. P. Ternovskii and G. D. Shnyrev: Determination of Young's modulus according to indentation diagram. Zavodskaya Laboratoriya. **41,** 1137 (1975).

11. M. F. Doerner and W. D. Nix: A method for interpreting the data from depth-sensing indentation instruments. Journal of Materials Research. **1,** 601 (1986).

12. W. C. Oliver and G. M. Pharr: An improved technique for determining hardness and

elastic-modulus using load and displacement sensing indentation experiments. Journal of Materials Research. **7,** 1564 (1992).

13. D. Penumadu, A. Dutta, G. M. Pharr and B. Files: Mechanical properties of blended single-wall carbon nanotube composites. Journal of Materials Research. **18,** 1849 (2003).

14. J. Alcala, F. Gaudette, S. Suresh and S. Sampath: Instrumented spherical micro-indentation of plasma-sprayed coatings. Materials Science and Engineering A - Structural Materials Properties Microstructure and Processing. **316,** 1 (2001).

15. A. Lau, M. L. Oyen, R. W. Kent, D. Murakami and T. Torigaki: Indentation stiffness of aging human costal cartilage. Acta Biomaterialia. **4,** 97 (2008).

16. E. A-Hassan, W. F. Heinz, M. D. Antonik, N. P. D'Costa, S. Nageswaran, C. A. Schoenenberger and J. H. Hoh: Relative microelastic mapping of living cells by atomic force microscopy. Biophysical Journal. **74,** 1564 (1998).

17. M. Stolz, R. Raiteri, A. U. Daniels, M. R. VanLandingham, W. Baschong and U. Aebi: Dynamic elastic modulus of porcine articular cartilage determined at two different levels of tissue organization by indentation-type atomic force microscopy. Biophysical Journal. **86,** 3269 (2004).

18. J. M. Mattice, A. G. Lau, M. L. Oyen and R. W. Kent: Spherical indentation load-relaxation of soft biological tissues. Journal of Materials Research. **21,** 2003 (2006).

19. A. Delalleau, G. Josse, J. M. Lagarde, H. Zahouani and J. M. Bergheau: Characterization of the mechanical properties of skin by inverse analysis combined with the indentation test. Journal of Biomechanics. **39,** 1603 (2006).

20. S. J. Lai-fook, T. A. Wilson, R. E. Hyatt and J. R. Rodarte: Elastic-constants of inflated lobes of dog lungs. Journal of Applied Physiology. **40,** 508 (1976).

21. K. Miller, K. Chinzei, G. Orssengo and P. Bednarz: Mechanical properties of brain tissue in-vivo: experiment and computer simulation. Journal of Biomechanics. **33,** 1369 (2000).

22. T. Y. Tsui, W. C. Oliver and G. M. Pharr: Influences of stress on the measurement of mechanical properties using nanoindentation .1. Experimental studies in an aluminum alloy. Journal of Materials Research. **11,** 752 (1996).

23. K. L. Johnson, K. Kendall and A. D. Robert: Surface energy and the contact of elastic solids. Proceedings of the Royal Society of London A - Mathematical, Physical and Engineering Science. **324,** 301 (1971).

24. B. V. Derjaguin, V. M. NMuller and Y. P. Toporov: Effect of contact deformations on the adhesion of particles. Journal of Colloid Interface Science. **67,** 326 (1975).

25. D. A. Spence: The hertz contact problem with finite friction. Journal of Elasticity. **5,**

3 (1975).

26. C. A. Clifford and M. P. Seah: Modeling of nanomechanical nanoindentation measurements using an AFM or nanoindenter for compliant layers on stiffer substrates. Nanotechnology. **17,** 5283 (2006).

27. S. Sen, S. Subramanian and D. E. Discher: Indentation and adhesive probing of a cell membrane with AFM: Theoretical model and experiments. Biophysical Journal. **89,** 3203 (2005).

28. M. A. Hajji, T. A. Wilson and S. J. Lai-fook: Improved measurements of shear modulus and pleural membrane tension of the lung. Journal of Applied Physiology. **47,** 175 (1979).

29. R. B. King: Elastic analysis of some punch problems for a layered medium. International Journal of Solids and Structures. **23,** 1657 (1987).

30. Y. G. Jung, B. R. Lawn, M. Martyniuk, H. Huang and X. Z. Hu: Evaluation of elastic modulus and hardness of thin films by nanoindentation. Journal of Materials Research. **19,** 3076 (2004).

31. H. J. Gao, C. H. Chiu and J. Lee: Elastic contact versus indentation modeling of multilayered materials. International Journal of Solids and Structures. **29,** 2471 (1992).

32. J. Mencik, D. Munz, E. Quandt, E. R. Weppelmann and M. V. Swain: Determination of elastic modulus of thin layers using nanoindentation. Journal of Materials Research. **12,** 2475 (1997).

33. A. K. Bhattacharya and W. D. Nix: Analysis of elastic and plastic-deformation associated with indentation testing of thin-films on substrates. International Journal of Solids and Structures. **24,** 1287 (1988).

34. A. E. Giannakopoulos and S. Suresh: Indentation of solids with gradients in elastic properties .2. Axisymmetric indentors. International Journal of Solids and Structures. **34,** 2393 (1997).

35. W. Li and T. Siegmund: Numerical study of indentation delamination of strongly bonded films by use of a cohesive zone model. Cmes-Computer Modeling in Engineering & Sciences. **5,** 81 (2004).

36. ABAQUS Theory manual, version 6.2. (Hibbitt, Karlsson and Sorensen Inc, Pawtucket, R.I., 2001).

37. R. Szilard: Theory and analysis of plates: classical and numerical methods. (Prentice-Hall, Englewood Cliffs, N.J.,, 1973).

38. E. H. Lee and J. R. M. Radok: Contact problem for viscoelastic bodies. Journal of Applied Mechanics. **27,** 438 (1960).

39. M. A. Hajji: Indentation of a membrane on an elastic half space. Journal of Applied Mechanics-Transactions of the Asme. **45,** 320 (1978).

40. A. Gouldstone, R. E. Brown, J. P. Butler and S. H. Loring: Stiffness of the pleural surface of the chest wall is similar to that of the lung. Journal of Applied Physiology. **95,** 2345 (2003).

41. I. N. Sneddon: The relation between load and penetration in the axisymmetric Boussinesque problem for a punch of arbitrary profile. International Journal of Engineering Science. **3,** 47 (1965).

42. W. H. Yang and K. H. Hsu: Indentation of a circular membrane. Journal of Applied Mechanics - Transactions of the Asme. **38,** 227 (1971).

43. S. Timoshenko and J. N. Goodier: Theory of elasticity. 3d ed. (McGraw-Hill, New York,, 1969).

44. M. A. Hajji, *Indentation of a membrane on an elastic half space with application to material testing of inflated lung lobes*. 1978, University of Minnesota.

45. A. C. Ugural: Stresses in plates and shells. 2nd ed. (McGraw Hill, Boston, 1999).

46. D. Stamenovic: Mechanical-properties of pleural membrane. Journal of Applied Physiology. **57,** 1189 (1984).

47. H. T. Xu and G. M. Pharr: An improved relation for the effective elastic compliance of a film/substrate system during indentation by a flat cylindrical punch. Scripta Materialia. **55,** 315 (2006).

48. A. Perriot and E. Barthel: Elastic contact to a coated half-space: Effective elastic modulus and real penetration. Journal of Materials Research. **19,** 600 (2004).

49. C. H. Hsueh and P. Miranda: Master curves for Hertzian indentation on coating/substrate systems. Journal of Materials Research. **19,** 94 (2004).

50. M. T. Huber: On the theory of the contact of solid elastic substrates. Annalen der Physik. **14,** 153 (1904).

51. S. Fuchs: Main strain trajectories from the contact of an orb with a disk. Physikalische Zeitschrift. **14,** 1282 (1913).

52. W. B. Morton and L. J. Close: Notes on Hertz's theroy of elastic bodies. Philosophical Magazine. **43,** 320 (1922).

53. G. M. Hamilton and L. E. Goodman: Stress field created by a circular sliding contact. Journal of Applied Mechanics - Transactions of the Asme. **33,** 371 (1966).

54. G. M. Hamilton: Explicit equations for the stresses beneath a sliding spherical

contact. Proceedings of the Institution of Mechanical Engineers Part C - Journal of Mechanical Engineering Science. **197,** 53 (1983).

55. I. Pane and E. Blank: Response to loading and stiffness of coated substrates indented by spheres. Surface & Coatings Technology. **200,** 1761 (2005).

56. D. Maugis: Contact, adhesion, and rupture of elastic solids. (Springer, Berlin, 2000).

57. H. Neuber: Kerbspannungslehre; grundlagen für genaue spannungsrechnung. (J. Springer, Berlin,, 1937).

Appendix

Appendix 1

Modification constant b in Eq. (4.6)

$$b = A_1 - \frac{A_2}{(1 + A_3 \cdot T_o(1-\nu)/\mu)^{1/A_4}}$$

where
A_1 = 1.1113
A_2 = 0.1122
A_3 = 7.7826
A_4 = 1.7131

Appendix 2

$I_1(r^o)$, $I_2(r^o)$, $L_1(r^o)$, $L_2(r^o)$, M in Eqs (4.22~26)

$$I_1(r^o) = \int_0^\infty \frac{\left[\int_0^1 \left(1-\frac{r^{o2}}{b^2}\right)^{1/2} r^o J_o(kr^o)dr^o\right]}{[1+\varepsilon k]} J_o(kr^o)dk$$

(b is modification factor in Appendix 1)

$$I_2(r^o) = \int_0^\infty \frac{\left[\int_0^1 \left(1-\frac{r^{o2}}{b^2}\right)^{1/2} r^o J_o(kr^o)dr^o\right]}{[1+\varepsilon k]} kJ_o(kr^o)dk$$

$$L_1(r^o) = \int_0^\infty \frac{J_1(k)}{k[1+\varepsilon k]} J_o(kr^o)dk$$

$$L_2(r^o) = \int_0^\infty \frac{J_1(k)}{k[1+\varepsilon k]} kJ_o(kr^o)dk$$

$$M = \int_0^1 \left(1-\frac{r^{o2}}{b^2}\right)^{1/2} 2\pi r^o dr^o$$

$$\varepsilon = \frac{T_o}{\mu a}(1-\nu)$$

$$p_o = \frac{4a\mu}{\pi R(1-\nu)}$$

Appendix 3

Displacement and stress distribution underneath indenter

$$u_{r^o}(r^o, z^o) = -(1-2\nu)\int_0^\infty e^{-kz^o}\beta(k)J_1(kr^o)dk + z^o\int_0^\infty ke^{-kz^o}\beta(k)J_1(kr^o)dk$$

$$u_{z^o}(r^o, z^o) = 2(1-\nu)\int_0^\infty e^{-kz^o}\beta(k)J_0(kr^o)dk + z^o\int_0^\infty ke^{-kz^o}\beta(k)J_0(kr^o)dk$$

$$\tau_{z^o z^o}(r^o, z^o) = -2\int_0^\infty ke^{-kz^o}\beta(k)J_0(kr^o)dk - 2z^o\int_0^\infty k^2e^{-kz^o}\beta(k)J_0(kr^o)dk$$

$$\tau_{r^o r^o}(r^o, z^o) = -2\int_0^\infty ke^{-kz^o}\beta(k)J_0(kr^o)dk + 2z^o\int_0^\infty k^2e^{-kz^o}\beta(k)J_0(kr^o)dk$$

$$-\frac{2z^o}{r^o}\int_0^\infty ke^{-kz^o}\beta(k)J_1(kr^o)dk + \frac{2(1-2\nu)}{r^o}\int_0^\infty e^{-kz^o}\beta(k)J_1(kr^o)dk$$

Here,

$$\beta(k) = -\frac{p_o}{2\mu[1+\varepsilon k]}\int_0^1\left(1-\frac{r^{o2}}{b^2}\right)^{1/2} r^o J_o(kr^o)dr^o - \frac{1}{2\mu}\left(C + 2\frac{T_o}{R}\right)\frac{J_1(k)}{k[1+\varepsilon k]}$$